

New Analyses of Star-to-Star Abundance Variations Among Bright Giants in the Mildly Metal-Poor Globular Cluster M5¹

Inese I. Ivans^{2,3}, Robert P. Kraft⁴, Christopher Sneden², Graeme H. Smith⁴, R. Michael Rich⁵, Matthew Shetrone⁶

ABSTRACT

We present a chemical composition analysis of 36 giant stars in the mildly metal-poor ($\langle[\text{Fe}/\text{H}]\rangle = -1.21$) globular cluster M5 (NGC 5904). The analysis makes use of high resolution data acquired for 25 stars at the Keck I telescope, as well as a re-analysis of the high resolution spectra for 13 stars acquired for an earlier study at Lick Observatory. We employed two analysis techniques: one, adopting standard spectroscopic constraints, including setting the surface gravity from the ionization equilibrium of iron, and two, subsequent to investigating alternative approaches, adopting an analysis consistent with the non-LTE precepts as recently described by Thévenin & Idiart. The abundance ratios we derive for magnesium, silicon, calcium, scandium, titanium, vanadium, nickel, barium and europium in M5 show no significant abundance variations and the ratios are comparable to those of halo field stars. However, large variations are seen in the abundances of oxygen, sodium and aluminum, the elements that are sensitive to proton-capture nucleosynthesis. These variations are well-correlated with the CN bandstrength index S(3839). Surprisingly, in M5 the dependence of the abundance variations on $\log g$ is in the opposite sense to that discovered in M13 by the Lick-Texas group where the relationship provided strong evidence in support of the evolutionary scenario. The present analysis of M5 giants does not necessarily rule out an evolutionary scenario, but it provides no support for it either. In comparing the abundances of M5 and M4 (NGC 6121), another mildly metal-poor ($\langle[\text{Fe}/\text{H}]\rangle = -1.08$) globular cluster, we find that silicon, aluminum, barium and lanthanum are overabundant in M4 with respect to what is seen in M5, confirming and expanding the results of previous studies. In comparing the abundances between these two clusters and others having comparable metallicities, we find that the anti-correlations observed in M5 are similar

²Department of Astronomy and McDonald Observatory, University of Texas, RLM 15.308, Mail Code c1400, Austin, TX 78712; iivans@astro.as.utexas.edu; chris@verdi.as.utexas.edu

³Research School of Astronomy & Astrophysics, Australian National University, Mount Stromlo Observatory, Cotter Road, Weston ACT 2611, Australia

⁴UCO/Lick Observatory, University of California, Santa Cruz, CA 95064; kraft@ucolick.org; graeme@ucolick.org

⁵Dept. of Physics & Astronomy, UCLA, Math-Sciences 8979, Los Angeles, CA 90095-1562; rmr@astro.ucla.edu

⁶McDonald Observatory, University of Texas, HC 75, Box 1337 L, Fort Davis, TX 79734; shetrone@astro.as.utexas.edu

to those found in more metal-poor clusters, M3, M10 and M13 ($\langle[\text{Fe}/\text{H}]\rangle = -1.5$ to -1.6), whereas the behavior in M4 is more like that of the more metal-rich globular cluster M71 ($\langle[\text{Fe}/\text{H}]\rangle \sim -0.8$). We conclude that among stars in Galactic globular clusters, there is no definitive “single” value of $[\text{el}/\text{Fe}]$ at a given $[\text{Fe}/\text{H}]$ for at least some alpha-capture, odd-Z and slow neutron-capture process elements, in this case, silicon, aluminum, barium and lanthanum.

Subject headings: Galaxy: abundances — globular clusters: general — globular clusters individual (NGC 5904) — stars: abundances — stars: fundamental parameters

1. Introduction

Large star-to-star abundance variations in the light elements C, N, O, Na, Mg, and Al are commonly found among the bright giant stars of metal-poor globular clusters. Some star-to-star abundance variations exist in all metal-poor globular clusters in which the variations have been sought. In clusters with sufficiently large sample sizes, N is typically anti-correlated with O and C, Na is anti-correlated with O, and Al is anti-correlated with Mg. The reader is referred to reviews by Suntzeff (1993), Kraft (1994), Briley *et al.* (1994), Da Costa (1997), Wallerstein *et al.* (1997), and Sneden (1999, 2000) for detailed discussions of these abundance trends. Except for anti-correlated behavior of N with respect to O and C, halo field giants do not exhibit the variations in Na, Mg, and Al that are seen among globular cluster giants (Pilachowski *et al.* 1996a, Hanson *et al.* 1998, Gratton *et al.* 2000).

Most studies agree that the abundance anti-correlations found among cluster giants result from proton-capture nucleosynthesis that converts C and O into N, Ne into Na, and Mg into Al in and above the hydrogen-burning shells of evolved stars (see *e.g.*, Denissenkov *et al.* 1990; Cavallo & Nagar 2000 and references therein). However it is less clear whether the synthesis takes place in the giants we presently observe (the “evolutionary” scenario) or in a prior generation of more massive evolved stars (the “primordial” scenario) which selectively “polluted” the gas from which the present generation of stars was formed. Evidence mounts that both scenarios are needed: a typical cluster contains main sequence stars already imprinted with variations in these elements, as studies of main sequence stars in 47 Tuc and NGC 6752 dramatically illustrate (Briley *et al.* 1995, Gratton *et al.* 2001). These abundances may, however, be further modified when the stellar envelope is cycled through the H-burning shell as stars approach the red giant tip (see reviews by Briley *et al.* 1994, Kraft 2001 and references therein).

¹Based in part on observations obtained with the W. M. Keck Observatory, which is operated by the California Association for Research in Astronomy, Inc., on behalf of the University of California, the California Institute of Technology and the National Aeronautics and Space Administration.

In any given luminosity interval on the giant branch of a typical globular cluster, there are stars with a range of Na, O, Mg, and Al abundances, usually exhibiting the anti-correlations noted above. One possible expectation of the evolutionary scenario is that the distribution of these O and Na (or Mg and Al) abundances should change with advancing evolutionary state. Thus as evolution proceeds, one might expect to find relatively more stars with low O and Mg and fewer with high O and Mg, and correspondingly more with high Na and Al and fewer with low Na and Al. This is indeed the case for M13 (Kraft *et al.* 1997, Hanson *et al.* 1998), in which there are different mean O, Na, Mg, and Al abundances for stars above and below $M_V^o \simeq -1.7$ (or $\log g \simeq 1.0$), a point 0.8 mag below the red giant tip. For other clusters less is known because of flux limitations at faint magnitudes. But even in M13, giants with $M_V^o > -1.7$ exhibit the same spread and distribution of Na and Al abundances (Pilachowski *et al.* 1996b, Cavallo & Nagar 2000), independent of luminosity, to levels one magnitude below the horizontal branch (HB). In the more metal-poor clusters M92 and M15, there is no apparent change in the distribution of Na abundances with luminosity from the red giant tip to levels just above the HB (Sneden *et al.* 2000). In the more metal-rich cluster M4, although the variations in C, N, O, Na, Mg, and Al are smaller than in M13, again the distributions show little dependence on evolutionary state (Ivans *et al.* 1999, hereafter called I99-M4).

M5 is a mildly metal-poor cluster ($\langle[\text{Fe}/\text{H}]\rangle = -1.4$, Zinn & West 1984; $\langle[\text{Fe}/\text{H}]\rangle = -1.17$, Sneden *et al.* 1992; $\langle[\text{Fe}/\text{H}]\rangle = -1.11$, Carretta & Gratton 1997) in which bright giants exhibit anti-correlated behavior of C and O with respect to N (Smith *et al.* 1997), as well as an anti-correlation of O with Na (Sneden *et al.* 1992, hereafter called S92-M5); Al and Mg abundance relationships have not been explored. The cluster exhibits bimodal distributions of CN-strength on both the first ascent giant branch (“RGB”; Smith & Norris 1983) and asymptotic giant branch (“AGB”; Smith & Norris 1993). At least one giant, IV-59, is known to have both high N and O, which again suggests the existence of primordial variations (Smith *et al.* 1997). However, is there evidence for an increase in the number of O-poor and Na-rich stars as evolutionary state advances? Previous M5 sample sizes have been too small to explore whether in this cluster a shift with M_V exists in the distribution of Na and O compatible with an evolutionary scenario. We report here an exploration of this question, based on high resolution spectra of a sample of 36 giants ranging in luminosity from the RGB tip to $M_V^o \sim -0.5$, *i.e.*, about one magnitude above the HB.

M4, a cluster with metallicity comparable to that of M5, has unusually high abundances of the α -element Si, the light odd-Z element Al, and the *s*-process elements Ba and La (Brown & Wallerstein 1992; I99-M4) in comparison to typical halo field giants of similar metallicity (see *e.g.*, Gratton & Sneden 1991, 1994, Shetrone 1996), which follow an extrapolation of the abundance trends seen among halo stars of lower metallicities (see *e.g.*, McWilliam *et al.* 1995, Ryan *et al.* 1996 and references therein). We therefore compare [el/Fe]-ratios in M5 with those in M4 and the halo field, noting that M5 pursues a galactic orbit with an apogalacticon in the outer reaches of the Galactic halo (Cudworth & Hanson 1993), where clusters having “abnormal” [el/Fe] ratios are sometimes found.

We introduce here for the first time an analysis of cluster [Fe/H] ratios based on an approach in

which allowance is made for the over-ionization of Fe in the atmospheres of low-metallicity giants. We estimate as well the effect of these non-local thermodynamic equilibrium (non-LTE) precepts on the derivation of [el/Fe] ratios. Abundances based on more traditional methods of analysis are, however, retained so that the reader may judge the extent of the proposed modifications.

2. Observations, Reductions and EW Measurements

Our prior study of 13 bright M5 giants (S92-M5) was based on high resolution ($R \sim 30,000$) spectra obtained with the Lick 3.0m telescope and Hamilton coude echelle spectrograph (Vogt 1987). The faintest stars observed in the Lick sample had $V \sim 13.0$, the practical limit for observations with signal-to-noise $S/N \gtrsim 50$ in reasonable integration times (~ 120 minutes) using the 3.0m telescope. However, stars near $M_V^o \sim -0.5$ have $V \sim 14.0$ in M5; obtaining spectra of high resolution and adequate S/N for such stars required use of the HIRES spectrograph of the Keck I telescope (Vogt *et al.* 1994).

For the Keck observations, the entrance slit was set to a width of $0.86''$, which corresponds to a spectral resolving power of $R \simeq 45,000$ at the Tektronix 2048×2048 pixel detector. In Table 1, we present an observing log of the 25 M5 giants observed with HIRES, along with estimated S/N near $\lambda 6300 \text{ \AA}$, values of V^o , $(B-V)^o$ and M_V^o for each star, assuming a reddening $E(B-V) = 0.03$ and a true distance modulus $(m-M)^o = 14.40$ (Djorgovski 1993). We adopted the observed colors and magnitudes of Sandquist *et al.* (1996; 2000, private communication) for all but three stars which were unobserved in the Sandquist *et al.* study. The photometry for star II-9 was taken from Cudworth (1979) and for star III-149, we used that of Rees (1993). G2 is discussed below.

Two of the stars observed at Lick (II-85 and IV-47) were re-observed using HIRES at Keck I, in order to study possible systematic offsets in equivalent width (EW) and/or differences in analysis procedure between the Lick and Keck data. Combining the two data sets, we are able to study abundances and abundance ratios in 36 M5 giants on both the RGB and AGB, ranging in luminosity from $M_{bol} \simeq -1.0$ to -3.4 , corresponding to an effective temperature range of $T_{\text{eff}} \simeq 4750 \text{ K}$ to 3900 K . Of these 36 stars, 34 are proper motion members of M5 according to the catalog of Rees (1993); the remainder have colors, magnitudes, abundances, and radial velocities compatible with membership (discussed further in the next paragraph). Eight of the stars are members of the AGB; a small fraction of stars brighter than $V = 12.8$ ($\sim 20\%$, based on comparative lifetimes), in the region of the color-magnitude diagram where the RGB and AGB cannot be distinguished, may also be AGB members. Of 30 stars observed by us for which the CN strength index S(3839) has previously been measured by Smith & Norris (1983, 1993), Briley & Smith (1993), and Smith *et al.* (1997), we observed 14 CN-strong stars and 16 CN-weak stars. Altogether, we observed 29% of the 118 giants brighter than $V = 14.1$ that were cataloged by Rees, plus two additional members not in the catalog. Our sample is thus reasonably representative of the population of bright M5 giants. In Figure 1 we exhibit the color-magnitude array of the brighter stars in M5, based on the CCD photometry of Sandquist *et al.* (1996; 2000, private communication). This figure illustrates

the evolutionary domain of our program stars. The labels in the figure identify the stars of this study plus those of S92-M5.

Two stars listed in Table 1 require special comment. The one designated as G2, close to the central region of the cluster, is not to be found in published photometry but was revealed as a bright red star in a $2\mu\text{m}$ image of the cluster kindly obtained by Kirk Gilmore using the Lick 1.0m telescope. G2 can be seen in the map (Figure 12) of Buonanno *et al.* (1981) and its estimated position is $\alpha(1950) = 15^{\text{h}}16^{\text{m}}04^{\text{s}}$, $\delta(1950) = +02^{\circ}14'54''$. It is a radial velocity member. A second star, listed here as “III-149” to prevent confusion, was accidentally observed in the mistaken belief that it was III-147. It is actually the star, not numbered in Buonanno *et al.*, lying $10''$ west and $4''$ south of III-147, essentially at the right-hand edge of Figure 12 of Buonanno *et al.* It too is a radial velocity member of M5.

Processing of the raw spectra was carried out using the standard IRAF software package⁷. The CCD frames were corrected for both bias and flat-field effects and the individual orders were extracted. Further analysis was performed using the SPECTRE code (Fitzpatrick & Sneden 1987); this involved continuum placement and normalization, cosmic ray removal, a wavelength calibration using stellar absorption lines within each order and removal of telluric absorption features using spectra of hot, rapidly-rotating, essentially featureless stars. The interested reader will find additional details of our standard procedures in earlier papers by this group (see *e.g.*, Sneden *et al.* 1991, I99-M4).

Our nominal HIRES wavelength coverage is $5400 \text{ \AA} \leq \lambda \leq 6700 \text{ \AA}$, but the free spectral ranges of the echelle orders are larger than can be recorded by the 2048×2048 pixel detector, so that features of some key elements are inevitably lost in the order interstices. In the 1994/5 observations, the grating was set to permit both Al I and Mg I lines to be recorded in a study of M13 giants. Unfortunately, the radial velocities of M5 and M13 are sufficiently different that for the M13 grating setting, lines of Mg I in M5 were shifted into the region between orders, and were therefore not recorded.⁸ On the other hand, the grating setting employed for the 1998 observations of M5 permitted observations of the Mg I lines, but not the Al I lines.

We measured EWs for all lines of interest by one of two techniques: direct integration of the flux across the observed line profile, or by adopting the EW of a Gaussian profile fitted to the line. The lines chosen for analysis in the $\lambda 5500 \text{ \AA}$ to $\lambda 6750 \text{ \AA}$ wavelength interval and their adopted gf -values are the same as those used in the previous paper of this series (I99-M4). We list the atomic parameters and corresponding reference for each line in Table 10 in the Appendix, where further discussion of the linelist is to be found. EWs of all measured lines can be obtained electronically

⁷IRAF is distributed by the National Optical Astronomy Observatories, which are operated by the Association of Universities for Research in Astronomy, Inc., under cooperative agreement with the National Science Foundation.

⁸During the observing runs discussed here, the Mauna Kea skies were partially clouded, and observations therefore limited. It was deemed unwise in these conditions to shift back and forth between grating settings, depending on temporal variations in transparency.

by request to the authors. They are also available at the Astronomical Data Center (ADC) at NASA Goddard Space Flight Center (http://adc.gsfc.nasa.gov/adc/archive_search.html). For the Na I $\lambda\lambda 5682, 5688$ Å doublet we based the abundance of Na on a synthetic spectrum fit, rather than EW measurements, since the lines in question are blended with other metallic species. We also checked by spectrum synthesis the O result obtained from the EW measurements of the [O I] $\lambda\lambda 6300, 6364$ Å doublet, employing interpolated C and N abundances as a function of O from Smith *et al.* (1997). Our vanadium abundances are derived from blended-line EW computations of $\lambda\lambda 6275, 6285$ Å for which we employed well-determined hyperfine structure components from McWilliam (2001, private communication), which are slightly revised from those of McWilliam & Rich (1994), normalizing the gf -values to those adopted for these lines in previous studies by our group. Finally, following the same Ba abundance analysis that was performed in I99-M4, the blended-line EW analysis of the lines at $\lambda\lambda 5854, 6142, 6497$ Å includes both hyperfine and isotopic subcomponents adopted from McWilliam (1998). Similarly, in this study, we assume the solar abundance ratios among the $^{134-138}\text{Ba}$ isotopes in the calculations.

3. Abundance Analysis: Critique of the Input Parameter Selection Process

3.1. Standard Analysis Procedure

The preliminary analysis of the observational data from the Keck I HIRES spectrograph followed the standard procedure of our earlier M5 paper (S92-M5). In that study, the values of V and $(B - V)$ given by Cudworth (1979), and the relationship between $(B - V)^o$ color and T_{eff} that had been adopted by Cudworth were used to provide a first estimate of T_{eff} for each program star. The adopted color excess $E(B - V) = 0.03$ and true distance modulus $(m - M)^o = 14.03$ were those recommended by Sandage & Cacciari (1990). In the present analysis, we used the values of V and $(B - V)$ given by Sandquist *et al.* (1996; 2000, private communication). We adopted the same color excess but the revised true distance modulus of $(m - M)^o = 14.40$ (Djorgovski 1993) was employed in preliminary estimates of $\log g$ obtained using the relationship obtained by combining the gravitation law with Stefan’s law. In S92-M5, the bolometric corrections of Bell & Gustafsson (1978) were employed but here we interpolated G. Worthey’s bolometric corrections (1994, private communication), in order to be consistent with the previous paper of this series (see I99-M4 for details).

Armed with these preliminary estimates of T_{eff} and $\log g$, we employed the current version of the MOOG line analysis code (Snedden 1973) to compute abundances from EWs on a line-by-line basis. For the various choices of T_{eff} and $\log g$ we calculated trial model atmospheres generated with the MARCS code (Gustafsson *et al.* 1975). Anticipating from S92-M5 that $\langle [\text{Fe}/\text{H}] \rangle$ would be near -1.2 , we took our input metallicity at $[\text{Fe}/\text{H}] = -1.0$, in order to simulate an overall α -element enhancement relative to Fe of ~ 0.2 to 0.3 dex, since the models were originally calculated for $[\alpha/\text{Fe}] = 0.0$. A discussion of the validity of this approximation is found in Fulbright & Kraft

(1999).

Final model atmosphere parameters were determined, as before, by iteration, through satisfying the following requirements: (a) for T_{eff} , that the abundances of individual Fe I lines show no trend with excitation potential; (b) for microturbulent velocity v_t , that the Fe I abundances show no trend with EW; and (c) for $\log g$, that the $[\text{Fe}/\text{H}]$ abundance ratios derived from the Fe I and Fe II lines should not differ by more than 0.05 dex. The iterated model parameters are given in Table 2; the values listed for $[\text{Fe}/\text{H}]$ in the traditional approach are a mean of determinations based on Fe I and Fe II. It is important to note in the iterative process that the “final” values of T_{eff} and $\log g$ may be fairly different from the estimated “input” values. Once T_{eff} is set, $\log g$ is constrained by the necessity to force close agreement in the $[\text{Fe}/\text{H}]$ values determined from Fe I and Fe II. Alternatively, once a $\log g$ is found to satisfy the ionization equilibrium, the T_{eff} is constrained to force agreement in the Fe I abundances for lines of different excitation potentials. Finally there is the additional constraint that $[\text{Fe}/\text{H}]$ cannot be allowed to vary systematically over the range of T_{eff} and $\log g$ represented by the stars in the sample.

Inspection of the preliminary atmospheric parameters in Table 2 gives rise to concerns. First, giants lying in the same T_{eff} range (3900 K to 4300 K) as those studied in S92-M5 have $\langle \log g \rangle$ that is ~ 0.5 dex lower than the values given in that paper. The increase in $(m-M)^{\circ}$ from 14.03 to 14.40 should have instead lowered $\langle \log g \rangle$ by only 0.15 dex. Second, the mean $[\text{Fe}/\text{H}]$ ratio is 0.15 dex lower among the six AGB stars than among the 13 RGB stars. Thus for the AGB we derive $\langle [\text{Fe}/\text{H}] \rangle = -1.45 \pm 0.01$ ($\sigma = 0.03$), whereas for the RGB we derive -1.30 ± 0.01 ($\sigma = 0.04$). Since a real physical reduction in Fe abundance from the RGB to the AGB is surely not expected in stars of such low mass, the result clearly points to some inadequacy in our analysis procedure. We list the $[\text{el}/\text{Fe}]$ ratios derived in this traditional approach in the Appendix as Table 11 where the values of $[\text{el}/\text{Fe}]$ are those based on the mean of Fe I and Fe II abundances.

We also investigated our abundance results in the context of possible mass loss or chromospheric activity in the atmospheres of our giant stars. In all but two of the Keck spectra, H- α was just barely recorded on the blue edge of the chip. Stars I-20, G2, IV-81, IV-19, and III-149 all show some H- α emission in the blue wing. Of these stars, I-20 is apparently an AGB star; the rest are on the tip of the giant branch. Unfortunately, most of the Na D doublet is unrecorded for these stars (the spectra are cut off redward of the blue wing of Na D2). The two Keck spectra which are offset in wavelength from the rest do, however, have the Na D doublet recorded. Stars II-85 and IV-47, both on the tip of the giant branch, show core shifts in both Na D lines. With a very conservative error of $\pm 2 \text{ km s}^{-1}$, we derive for the D2 lines a shift of -9.8 km s^{-1} and for D1, -7.6 and -9.7 km s^{-1} , for stars II-85 and IV-47, respectively. That the bluer D2 line may show a slightly higher blueshift is in accord with its formation higher in the atmosphere, and is thus more susceptible to any outward flows in the higher atmosphere regions (see *e.g.*, Bates *et al.* 1993 and references therein).

3.2. A New Approach

“For many years, the techniques used in stellar abundance determinations have remained essentially unchanged, despite a rather passionate controversy in the late fifties and early sixties [...] that departures from LTE could lead to abundances substantially different from those given by the ‘classical’ LTE approach” (Dumont *et al.* 1975). Detailed investigations since have confirmed not only the effect on derived abundances but also on the derived stellar parameters (see *e.g.*, Hearnshaw 1976, Luck & Lambert 1985, Fuhrmann *et al.* 1997, Allende Prieto *et al.* 1999, Fulbright 2000, the latter three studies based on *Hipparcos* [ESA 1997] results). The largest effect on stellar parameters is on the derived gravity: gravities derived by forcing ionization equilibrium (spectroscopic gravity) are lower than those derived by stellar parallaxes (trigonometric gravity) or by the evolutionary position in the HR-diagram (evolutionary gravity). We confirm this gravity anomaly in our LTE analysis of the M5 giant stars and discuss the anomaly further in this section.

Recently, Thévenin & Idiart (1999, hereafter TI99) have explored in detail the problem of Fe over-ionization in the atmospheres of metal-poor stars. For over-ionized atmospheres, application of standard LTE model atmospheres to abundance analysis of Fe I will always lead to an underestimate of [Fe/H]. TI99 point out that at any given optical depth, the populations of the atomic levels of Fe I are governed not by the local kinetic temperature but rather are modified by the outward leakage of UV photons into an atmosphere made progressively less opaque as metallicity is decreased. The metallicity dependence is not surprising: it has been known for some time that for a given optical depth, lower metallicity stars have a larger physical depth (see *e.g.*, Wallerstein 1962) and the optical depth thus reaches hotter layers of the atmosphere. Fortunately, the abundance of Fe derived from Fe II remains relatively unaffected, since in metal-poor stars, virtually all Fe is already in the form of Fe II. The TI99 calculations suggest that the reduction of [Fe/H] estimated from Fe I relative to Fe II amounts to about 0.1 dex at [Fe/H] = -1.0 but rises to about 0.3 dex at [Fe/H] = -2.5 . For similar reasons, the leakage of UV photons should also become larger with lower atmospheric densities, *i.e.*, surface gravities, at a given T_{eff} , and with higher T_{eff} values at a given luminosity. Thus one might anticipate that should the TI99 effect be real, traditional analyses of AGB stars could well lead to lower overall estimates of [Fe/H] based on Fe I, as compared with RGB stars. A smaller, but still noticeable, “dragging down” of [Fe/H] would occur when [Fe/H] is estimated from the mean of Fe I and Fe II determinations. Could this effect account for the anomalous apparent drop in [Fe/H] among M5 AGB stars?

We decided to test this possibility in three ways: first, by modifying our Fe linelist to exclude all but the weakest lines; second, by modifying the linelist to exclude all but the highest excitation potential lines; and third, by modifying the procedure used to define the stellar parameters. By gradually culling the lines in descending order of equivalent width, we found a small but steady increase in the microturbulent velocity required to satisfy the EW equilibrium constraint but, no significant change in either the Fe I to Fe II ratio or in the overall iron abundance. Gradual deletions of lines in ascending order of excitation potential had no significant effect on the ratio or abundance and the changes in v_t were up or down, depending on the subset of lines in use in

a given trial. Finally, we modified our procedure for estimating the input values of T_{eff} and $\log g$ in the following way. First, we set aside any reference to the Fe I spectrum in estimating T_{eff} and replaced it with values of T_{eff} derived from $(B-V)^o$, using the calibration of Alonso *et al.* (1999; their Table 6, interpolating the computed table values).⁹ This scale, based on the Infra-Red Flux Method (“IRFM”; Blackwell *et al.* 1990 and references therein), applies to low-mass, metal-poor giants. We then assigned to each star the value of $\log g$ it should have, as predicted from stellar models coupled to stellar evolution. To each star on the RGB, we assigned a mass of $0.80 M_{\odot}$, and to each star on the AGB a mass of $0.70 M_{\odot}$, thus allowing for the mass loss expected in very late evolutionary stages. We took $E(B - V) = 0.03$, $(m-M)^o = 14.40$, and calculated $\log g$ from the relationship $g \sim \mathcal{M} \times T_{\text{eff}}^4 / L$, interpolating G.Worthey’s bolometric corrections (1994, private communication). The observed values of V and $(B - V)$ used in S92-M5 were replaced by modern CCD-based values of Sandquist *et al.* (1996; 2000, private communication).

In Table 2 we show a comparison of T_{eff} and $\log g$ values derived from the “traditional” approach based on the Fe I and Fe II line spectrum and the revised approach based on the Alonso *et al.* (1999) color versus T_{eff} -scale and stellar evolutionary arguments. For the 13 RGB stars and 6 AGB stars, we find $\delta T_{\text{eff}} = +26 \pm 10$ K and $\delta T_{\text{eff}} = +35 \pm 18$ K respectively, in the sense “new” *minus* “traditional”. The difference between T_{eff} based on the Fe I excitation plot and T_{eff} based on the Alonso *et al.* color- T_{eff} -scale is very small and the effect on the abundances of Fe derived from Fe I and Fe II is essentially negligible. Thus an increase in T_{eff} of 30 K increases $\log \epsilon(\text{Fe I})$ by 0.02 dex and decreases $\log \epsilon(\text{Fe II})$ by 0.04 dex. But the change in $\log g$ has a more substantial effect; we find $\delta \log g = +0.28 \pm 0.04$ for the RGB sample and virtually the same result, $\delta \log g = +0.34 \pm 0.06$ for the AGB sample, again in the sense “new” *minus* “traditional”. Such a gravity change tends to drive the derived Fe abundances from Fe I and Fe II apart: for $\delta \log g = +0.30$, we expect $\delta \log \epsilon(\text{Fe I}) \simeq -0.02$ and $\delta \log \epsilon(\text{Fe II}) \simeq +0.15$. These changes are qualitatively what one would expect if the TI99 conjecture were in fact true.

In Table 3 we tabulate the changes in $\log \epsilon(\text{Fe I})$ and $\log \epsilon(\text{Fe II})$ corresponding to small changes in the input parameters: T_{eff} , $\log g$, v_t , $[\text{Fe}/\text{H}]$, distance modulus, and stellar mass for a typical M5 RGB star: $T_{\text{eff}} = 4325$ K, $\log g = 1.08$, $v_t = 1.65$. From the arguments in the preceding paragraph plus inspection of this table, one can easily see the scope of the dilemma. The Fe I excitation plot yields essentially the same T_{eff} values as the Alonso *et al.* (1999) T_{eff} -scale, in turn based on the IRFM. It therefore seems unlikely this temperature scale is seriously in error. If the disagreement between the spectroscopic gravities, based on forced agreement between Fe I and Fe II abundances, and the evolutionary gravities is due to a defect in estimating the latter, then the evolutionary $\log g$ would need to be decreased by ~ 0.3 dex. This would in turn imply that the distance modulus of M5 is too small, and needs to be increased by 0.75 dex, *i.e.*, to $(m-M)^o = 15.15$. Such an increase in the distance modulus would be seriously at odds with recent estimates based on fitting of the M5

⁹We have since verified that the *corrected* version of the formula in the caption of Table 2 of Alonso *et al.* yields similar results.

main sequence to the main sequence of mildly metal-poor subdwarfs having accurate *Hipparcos*-based parallaxes. For example, Reid (1997) finds $(m-M)^o = 14.45$ from this approach, very close to the value adopted here. M5 also contains many RR Lyrae variables for which $\langle V^o \rangle = 15.02$ if $E(B - V) = 0.03$ (Jones *et al.* 1988). Assuming that halo field and globular cluster RR Lyraes are analogs of each other, these are expected to have $\langle M_V^o \rangle = +0.7 \pm 0.1$ (Layden *et al.* 1996, based on their Figure 7) in which case $(m-M)^o \sim 14.3$, again close to our assumed value. A modulus of 15.15 would cause the RR Lyraes of M5 to be unacceptably bright.

Returning to Table 2, we tabulate values of $[\text{Fe}/\text{H}]$ determined independently from Fe II and Fe I, based on our revised procedure. We now *assume* that $[\text{Fe}/\text{H}]$ is correctly given by the Fe II value. In that case, for the 13 RGB stars, $\langle [\text{Fe}/\text{H}] \rangle = -1.20 \pm 0.01$, ($\sigma = 0.04$) and for the 6 AGB stars, $\langle [\text{Fe}/\text{H}] \rangle = -1.26 \pm 0.04$ ($\sigma = 0.07$). In comparison to the results from the “traditional” analysis, the difference in Fe abundance between the AGB and RGB has been reduced from 0.15 to 0.06 dex; the latter difference is close to a $1\text{-}\sigma$ combined error and thus is acceptable. The over-ionization of Fe follows from a comparison of $[\text{Fe}/\text{H}]$ determined from Fe I and Fe II. Thus for the 13 RGB stars, $\langle \delta[\text{Fe}/\text{H}] \rangle = -0.09 \pm 0.01$ ($\sigma = 0.05$) and for the 6 AGB stars, $\langle \delta[\text{Fe}/\text{H}] \rangle = -0.18 \pm 0.03$ ($\sigma = 0.08$), in the sense Fe I *minus* Fe II.¹⁰ As anticipated, the depression of Fe I abundances relative to those of Fe II is more severe for AGB stars as compared to RGB stars. In Figures 2, 3 and 4, we illustrate the difference, $\delta \log \epsilon(\text{Fe}) = \log \epsilon(\text{Fe I}) - \log \epsilon(\text{Fe II})$, as functions of T_{eff} (Alonso *et al.* 1999) and $\log g$ (evolutionary), as well as $\log \epsilon(\text{Fe II})$ as a function of T_{eff} for all of our program stars.¹¹ One AGB star (I-20) remains somewhat anomalous in having an unusually low Fe II abundance; we return to this star later.

3.3. Alternative Approaches

In the preceding, we adopted the T_{eff} -scale of Alonso *et al.*, which follows an empirical approach based on the IRFM. However, examining the offsets in Fe abundance exhibited in Table 3, we see that agreement between $\log \epsilon(\text{Fe I})$ and $\log \epsilon(\text{Fe II})$ could also be achieved if we increased T_{eff} by $\sim 60\text{K}$ and $\sim 120\text{K}$ for RGB and AGB stars (along with accompanying small increases in $\log g$), respectively. However, from Table 2, we see that adoption of these increases would exacerbate the difference between the T_{eff} obtained from the Fe I excitation plot and the newly corrected T_{eff} , by $+72\text{K}$ and $+160\text{K}$ for RGB and AGB stars.

T_{eff} -scales other than that of Alonso *et al.* (1999) can be found in the literature. A recent version is that of Gratton *et al.* (2000). We can compare values of T_{eff} using metal-poor giants

¹⁰Adoption of the larger distance modulus of 14.62, based on Hipparcos subdwarfs, favored by Gratton *et al.* (1997), reduces slightly the differences between $[\text{Fe}/\text{H}]$ based on Fe I and $[\text{Fe}/\text{H}]$ based on Fe II. For the 13 RGB and 6 AGB stars, the differences become -0.06 and -0.15 dex, respectively. The difference of the differences remains, of course, the same.

¹¹These figures include the entire sample of stars discussed in this paper. See also §6.

common to the two investigations; there are five such field giants shared between Gratton *et al.* (2000) and Alonso *et al.* (1999), from which we find $\delta T_{\text{eff}} = +71\text{K} \pm 68\text{K}$, with the Gratton *et al.* scale the hotter of the two. However, conflicting evidence is found from a study of near-UV fluxes and flux distributions of metal-poor stars by Allende Prieto & Lambert (2000). Their investigation contains 15 stars in common with Alonso *et al.* (1996) and having $[\text{Fe}/\text{H}] < -0.5$ with $4000\text{K} \leq T_{\text{eff, Alonso}} \leq 6000\text{K}$ (omitting the spectroscopically peculiar dwarfs HD134439 and HD25329). For these 15 stars we find a negligible offset of $\delta T_{\text{eff}} = +32\text{K} \pm 56\text{K}$, in the sense UV *minus* IRFM. Unfortunately, the sample consists entirely of dwarfs. Allende Prieto & Lambert also compare their UV-flux derived values of T_{eff} with those of Gratton *et al.* (2000). In this case, there are four giants in common (we omit the heavily reddened HD166161). For these four stars, we find a much larger offset of $\delta T_{\text{eff}} = +94\text{K} \pm 63\text{K}$, in the sense Gratton *et al.* *minus* Allende Prieto & Lambert.

We also investigated the effects of adopting the color- T_{eff} calibration of Sekiguchi & Fukugita (2000). For stars with temperatures that correspond to the warmer M5 stars in our sample, the Sekiguchi & Fukugita color- T_{eff} calibration produces temperatures $\sim 50\text{K}$ hotter than the other calibrations. This temperature shift improves the situation for our hottest AGB stars but also affects our warm RGB stars. On the other hand, for stars with temperatures that correspond to the coolest M5 stars in our sample, we find that their calibration produces a T_{eff} -scale that is $\sim 100\text{K}$ cooler than that of the Alonso *et al.* (1996) calibration, a temperature difference that is in agreement with the overall findings of Sekiguchi & Fukugita. Thus, the overall effect of the Sekiguchi & Fukugita T_{eff} -scale is to change the slope of the T_{eff} vs $\log g$ relationship to one which is in the *opposite* sense of what is required to correct the cool AGB versus RGB + “tip” star iron abundances. In summary, these comparisons clearly offer no firm evidence that the Alonso *et al.* T_{eff} -scale requires any upward revision.

In an alternative approach, we abandon the Alonso *et al.* IRFM-based T_{eff} scale and instead derive T_{eff} and $\log g$ from the comparison of observed and synthetic colors of models for low-mass, metal-poor giants. New models have recently been calculated by Houdashelt *et al.* (2000), in which values of $(B - V)$, $(V - K)$, (and other colors) are given as a function of T_{eff} and $\log g$ for metal abundances ranging from solar to $[\text{Fe}/\text{H}] = -3$. To determine whether adoption of these models would in some way modify our conclusions, we considered a sample of M5 giants drawn from our Table 1, distributed so that RGB, AGB and “tip” stars are all represented. We then calculated T_{eff} and $\log g$ for each star, entering the Houdashelt *et al.* tables with the observed values of $(B - V)^o$, and assuming as before a true distance modulus of 14.40. The BC’s adopted in this case were those of Houdashelt *et al.*. Unfortunately, this procedure proved difficult to apply in practice for two reasons. First, the expected metallicity of M5 is in the range $[\text{Fe}/\text{H}] = -1.2$ to -1.35 , and the Houdashelt *et al.* tables contain entries only for $[\text{Fe}/\text{H}] = -1.0$ and -2.0 . Thus one must interpolate within the framework of a rather coarse grid. Second, at a fixed $(B - V)$, the relationship between T_{eff} and $[\text{Fe}/\text{H}]$ is non-linear, so that linear interpolation at the metallicity of M5 is not adequate. However, these difficulties can be overcome by employing $(V - K)^o$ as the independent variable, since T_{eff} is practically independent of $[\text{Fe}/\text{H}]$ at a fixed value of $(V - K)^o$, and depends very little

on $\log g$. To obtain $(V-K)^o$ for the stars in our Keck sample, we plotted $(B-V)^o$ vs $(V-K)^o$ for the 25 stars observed by Frogel *et al.* (1983), and used this plot to transform $(B-V)^o$ to $(V-K)^o$, retaining the more recently acquired V magnitudes and $(B - V)$ colors of Sandquist (1996; 2000, private communication). The color-color plot proved to be extremely tight: we estimate that the transformation could introduce an error of no more than 0.01 mag in $(V-K)^o$. This procedure permitted us to estimate values of T_{eff} with little uncertainty due to errors in interpolation.

The difference between T_{eff} derived from the Houdashelt *et al.* models and T_{eff} derived from the Alonso *et al.* scale is shown as a function of M_V^o in Figure 5. The difference shows a steady increase with luminosity from \sim zero at $M_V^o = -0.5$ to $\sim +60\text{K}$ at $M_V^o = -2.5$. Results and comparisons with entries in Table 2 are shown in Table 4. The Houdashelt *et al.* values of T_{eff} are higher than the Alonso *et al.* IRFM-based values of T_{eff} by average offsets of $27\text{K} \pm 21\text{K}$ for the three RGB stars, $+60\text{K} \pm 10\text{K}$ for the three “tip” stars, and $+43\text{K} \pm 20\text{K}$ for the three AGB stars (also see Figure 5). Within the errors, the offsets in T_{eff} appear comparable (the overall average is $+43\text{K} \pm 20\text{K}$). However, using the higher values of T_{eff} , the average offsets in the iron abundances, $\delta[\text{Fe}/\text{H}] = \log \epsilon(\text{Fe I}) \textit{ minus } \log \epsilon(\text{Fe II})$, become -0.06 ± 0.02 , -0.07 ± 0.06 , and -0.16 ± 0.07 for the same three groups of stars. Regardless of which of the preceding T_{eff} -scales we adopt, the abundance of Fe based on Fe II remains essentially constant with evolutionary state, whereas $[\text{Fe}/\text{H}]$ based on Fe I remains significantly smaller on the AGB as compared with the RGB and “tip” stars. Simply adopting the hotter T_{eff} -scale of Houdashelt *et al.* for the sample does not solve the overall problem of over-ionization.

As to additional sources of systematic differences between Fe I vs Fe II abundances, the referee noted that the gf -value zero-point for Fe II is possibly not as well known as one would like. Two recent studies of Fe II gf -values, those of the “critical compilation” of the NIST Atomic Spectra Database (Version 2.0; <http://physics.nist.gov/asd>; Martin *et al.* 1999) and Schnabel *et al.* (1999) provide lines in common with those shown in the Appendix (Table 10). The difference between our values and the NIST values is $+0.10 \text{ dex} \pm 0.09 \text{ dex}$, in the sense of M5 *minus* NIST. Adopting the NIST $\log gf$ -values would produce an even larger disagreement between our Fe I and Fe II abundances. With the Schnabel *et al.* (1999) linelist, our two lines in common have a difference in the $\log gf$ -values of $-0.14 \text{ dex} \pm 0.09 \text{ dex}$, in the sense of this study *minus* Schnabel *et al.* However, the solar abundance of iron derived using the Schnabel *et al.* linelist is 7.42, not the 7.52 we have adopted here and in our previous work. Normalizing the Schnabel *et al.* lines to reproduce our adopted solar abundance would negate the offset that the lines would otherwise generate. While an increase in the $\log gf$ -values of Fe II by 0.1 dex from those which we have employed in our previous Lick-Texas work would indeed bring the “tip” and RGB giant $[\text{Fe}/\text{H}]$ values for Fe I and Fe II into agreement using the Alonso *et al.* T_{eff} -scale, any change “across the board” in Fe II gf -values would not simultaneously satisfy the Fe I vs Fe II offsets for the AGB stars.

We summarize the findings of this section by noting that one of three procedural choices can be adopted:

1. We adopt the traditional methods of high resolution spectroscopy, including setting the surface gravity from the ionization equilibrium of iron, in which case we find that the mean $[\text{Fe}/\text{H}]$ value decreases by 0.15 dex as stellar evolution advances from the RGB to the AGB.
2. We abandon the traditional approach using spectroscopic constraints, basing the analysis instead on values of T_{eff} derived from the Alonso *et al.* (1999) relation between $(B - V)$ and T_{eff} , which is in turn based on the Infra-Red Flux Method (Blackwell *et al.* 1990 and references therein), and values of $\log g$ derived from application of stellar evolution plus knowledge of the cluster distance modulus. This approach stabilizes the Fe II abundance as a function of evolutionary state but requires acceptance of the idea that Fe I is over-ionized and out of equilibrium with Fe II, consistent with the non-LTE precepts described by Thévenin & Idiart (1999). The over-ionization of Fe I turns out to be more severe among AGB as compared with RGB stars. Interestingly, this T_{eff} -scale is in close agreement with the T_{eff} -scale derived from the Fe I excitation vs EW plot.
3. An alternative solution requires arbitrarily increasing the values of T_{eff} above the Alonso *et al.* scale by $\sim 60\text{K}$ on the RGB and $\sim 120\text{K}$ on the AGB; these changes would bring Fe I and Fe II abundances nearly into agreement. The recent models of metal-poor stars by Houdashelt *et al.* (2000), which predict $(B - V)$, $(V - K)$, and other colors from T_{eff} and $\log g$ for different choices of $[\text{Fe}/\text{H}]$, do indeed predict higher values of T_{eff} than those of the Alonso *et al.* scale. Why the models give a T_{eff} vs color scale that is hotter than the scale based on the IRFM is not clear. The Houdashelt *et al.* models come close to satisfying ionization constraint requirement among the RGB stars, but are still too cool by $\sim 70\text{K}$ to rectify the situation for AGB stars. And, if we make the AGB stars 120K hotter than the Alonso *et al.* (1999) scale, the abundance of Fe II will drop to a level about 0.1 dex lower than its value among RGB stars.

Here we adopt procedure (2) as one extreme, and report the results of procedure (1), the opposite extreme, in the Appendix. The reader should bear in mind that the “intermediate” solution under (3) remains an option, but requires a fairly large systematic correction to the IRFM-based T_{eff} -scale and a smaller, but still significant, correction to the T_{eff} -scale based on the Houdashelt *et al.* models.

4. $[\text{el}/\text{Fe}]$ Ratios: A Rationale

Based on the revised approach, the determination of $[\text{el}/\text{Fe}]$ ratios becomes more complex than is the case in the traditional approach. If Fe is over-ionized, then one might expect a corresponding over-ionization of elements having first ionization potentials \lesssim to that of iron. In the yellow-red spectral regions of globular cluster giants, almost all detectable transitions arise from “metallic elements” that exist predominantly in singly ionized states. But aside from Fe, which has both neutral and ionized species lines available, only a few elements (*e.g.*, Sc, Ba, La, Eu, and sometimes

Ti) have observable transitions arising from their first ionized states in our stars. Fortunately, the $[\text{el}/\text{Fe}]$ ratios of these elements are confidently estimated from their $[\text{el}/\text{H}]$ ratios and $[\text{Fe}/\text{H}]$ ratios from Fe II. For the majority of elements with only neutral-species lines present, estimates must be made of the degree to which the neutral populations are depleted by over-ionization. Oxygen is a special case: it remains overwhelmingly neutral and in the ground state, shielded from over-ionization both by its very high first ionization potential (13.6 eV) and the opacity corresponding to the Lyman jump. There is little doubt that the $[\text{O}/\text{Fe}]$ ratio should be based on $[\text{Fe}/\text{H}]$ derived from Fe II.¹²

The degree of over-ionization of any particular species depends on the ionization potential, the term scheme and the location and strength of the absorption transitions of that atom in relation to the flux distribution of the excess UV photons. The excess UV photons envisaged by TI99 must have a complicated UV energy distribution reflecting the highly jagged opacity distribution longward of the Lyman limit. Calculating the degree of excess ionization is further complicated by the fact that ionizations can take place from excited levels as well as the ground state. To determine accurately the degree of over-ionization of those species which appear in our spectra only in the neutral state would require the calculation of collisional and radiative rates for thousands of levels, as was done in the case of Fe I and Fe II by TI99. Such calculations for similar elements are beyond the scope of this paper, although it is obvious that detailed studies need to be carried out.

In the absence of such theoretical calculations, we looked for guidance in the empirical domain, in particular among stars with values of $\log g$ similar to those of M5 giants, but having higher metallicities so that EWs of ionized lines of such species as Si, Ti, and V are large enough to be measured. A sample of LMC and SMC cepheids (Luck *et al.* 1998) provides $[\text{el}/\text{H}]$ ratios for neutral and ionized states of these three elements both for $\log g$ based on stellar evolution and for $\log g$ derived from the Fe I versus Fe II ionization balance. Whenever Fe appears to be over-ionized as a result of adopting an “evolutionary” $\log g$, these authors generally find that Si, Ti, and V are excessively ionized by essentially the same amount as is Fe.¹³ A similar over-ionization effect is found by Kovtykh & Andrievsky (1999) in δ Cep.

If this situation applies also in the M5 giants considered here, then the abundance ratios of $[\text{Si}/\text{Fe}]$, $[\text{Ti}/\text{Fe}]$, and $[\text{V}/\text{Fe}]$ can be estimated from the assumption that the degree of over-ionization of these species is the same as that of Fe. In that case these elements must be referenced to the abundance of Fe based on Fe I. In the absence of detailed calculations we broaden this procedure

¹²This statement does not take into account the possibility of a small effect induced by ionizations from the low-lying singlet S and D states of O I.

¹³Note that we are concerned here with *changes* in the ionization as a result of abandoning the ionization equilibrium of Fe as a means of setting $\log g$. Thus for example in the case of the SMC cepheid HV 837, Luck *et al.* find that $[\text{Fe II}/\text{Fe I}]$ increases from -0.01 to $+0.54$ as $\log g$ changes from -0.28 (spectroscopic) to $+0.82$ (evolutionary). The corresponding increases in $[\text{Ti II}/\text{Ti I}]$ are 0.00 to $+0.55$ and for $[\text{Si II}/\text{Si I}]$ are $+0.31$ to $+0.84$. The changes are essentially the same as for Fe. However, we note that when Fe is in equilibrium, Si is not.

to include all elements which present themselves in the neutral state except for oxygen, which for reasons already cited, we reference to Fe based on Fe II.

We summarize our estimates of the [el/Fe] ratios for the 19 RGB plus “tip” and 6 AGB stars in question in Table 5. Columns 3 and 4 contain the values of [Fe/H] estimated independently for $\log \epsilon(\text{Fe II})$ and $\log \epsilon(\text{Fe I})$ and column 5 contains [O/Fe], assuming that Fe II yields the correct abundance of Fe. For the remaining elements up through the Fe-peak group (except for Sc), we list [el/Fe] on the simple assumption that it is “correct” to ratio $\log \epsilon(\text{el I})$ to $\log \epsilon(\text{Fe I})$. For the heavy elements (and Sc), we ratio $\log \epsilon(\text{el II})$ to $\log \epsilon(\text{Fe II})$. Mean values of [el/Fe] are found at the bottom of Table 5, individually calculated for RGB and AGB stars. These should be compared with mean values from Table 11 in the Appendix, which are based on the “traditional” method of analysis.

5. Adopted [el/Fe] Ratios: the 25 Stars Observed with the Keck I HIRES

Following the arguments of the last two sections we assume that [el/Fe] ratios are properly deduced by referring neutral species abundances to Fe I and ionized species to Fe II, the only exception being [O/Fe] derived from [O I], which is referred to Fe II. Following this precept, we add to the 19 RGB and AGB giants of Table 5 the six stars near the red giant tip and display the resultant [el/Fe] ratios also in Table 5.

Table 5 lists the means of [Fe/H] derived from Fe II and Fe I, and the means for the [el/Fe] ratios based on the above discussion, where we have divided the material into four groups: 13 RGB, 6 AGB, 19 RGB plus “tip” stars and finally, all 25 stars observed with the Keck I HIRES. Except for the differences in [Fe/H] derived from Fe I versus Fe II, there are few surprises. O, Na, and Al abundances have a substantial spread of the kind exhibited by most globular clusters (see the reviews cited in §1), and the α -elements Si, Ca, and Ti have their usual abundance enhancements of $\sim +0.2$ to $+0.35$ dex. Sc, V, and Ni have [el/Fe] ratios not far from 0.0, [Mn/Fe] $\simeq -0.25$ as expected (see *e.g.*, McWilliam 1997), and the ratio [Ba/Eu] $\simeq -0.27$ is similar to that found in field giants (Shetrone 1996, McWilliam 1997) and field subdwarfs (Fulbright 2000, 2001) having the metallicity of M5.

Somewhat disconcerting is the slight run of [Ba/Eu] toward larger values in the most advanced evolutionary state – the AGB. That this is probably not a manifestation of slow neutron-capture nucleosynthesis occurring within the stars themselves follows from the fact that [La/Eu] exhibits the opposite behavior. The slight runs seen here in Ba are likely due to the choice of microturbulent velocity: the iron line constraint is satisfied but the same microturbulent velocity may not be appropriate for the atmospheric layers where the Ba lines are formed in the lower density AGB stars.

6. Re-analysis of the Earlier Lick Observations

The abundances reported by S92-M5 refer to 13 M5 giants observed with the Lick Hamilton Echelle, two of which (II-85 and IV-47) overlap with the 25 stars observed at Keck. Most of these 13 Lick stars lie near the RGB tip and therefore provide a valuable supplement to the Keck sample. The earlier analysis employed the “traditional” approach; we consider here a re-analysis of the same data based on our revised approach. Allowances must be made, however, for the lower spectral resolution and more limited free spectral range of the earlier Lick observations.

We first re-measured the Lick EW’s to be sure that continuum levels and line fitting procedures were consistent with the norms established in dealing with the Keck I observations. A plot of original versus re-measured Lick EWs is shown in Figure 6, from which it is clear that there is no significant difference between them. We then used the two stars that had been observed both at Keck I and Lick to compare the EW scales of their spectrographs. In Figure 7 we plot the difference between the Keck I and (re-measured) Lick EWs as a function of the Keck I EWs. The straight line fit illustrated in this figure indicates that the Lick EWs must be reduced systematically by 5% to get on the system defined by the Keck I HIRES spectrograph, that is $EW_{\text{Keck}} = 0.95 \times EW_{\text{Lick}} \pm 0.09 \text{ m}\text{\AA}$ ($\sigma = 6.1 \text{ m}\text{\AA}$) for the 42 lines of II-85 and the 51 lines of IV-47 in common between the data sets.¹⁴

In Table 6 we give the “new” values of T_{eff} , $\log g$, v_t , $[\text{Fe}/\text{H}]$ based on the abundances of Fe I and Fe II, and the $[\text{el}/\text{Fe}]$ ratios, all following the modified procedures outlined in §3.2, and employing the revised EWs discussed above, reduced by 5%. We omit star II-9 from further consideration: the S/N of the observed Lick spectrum we now consider unacceptably low. The combined Lick/Keck sample therefore contains 35 giants. The offsets between $\log \epsilon(\text{Fe I})$ and $\log \epsilon(\text{Fe II})$ for the entire sample, as functions of T_{eff} and $\log g$, are illustrated in Figures 2 and 3, and the corresponding $\log \epsilon(\text{Fe II})$ values are shown in Figure 4.

We compare the entries in Table 6 with the “all star” means of Table 5, since the Lick sample contains a mixed group of tip, RGB, and AGB stars. There are no differences in $[\text{Fe}/\text{H}]$ exceeding 0.03 dex, and no differences in $[\text{el}/\text{Fe}]$ ratios exceeding a 1- σ error except in the case of $[\text{Sc}/\text{Fe}]$ (derived from Sc II lines), where the difference approaches the 2- σ level. The Lick spectra also provided access to Sc I as well as Sc II lines. However, the $[\text{Sc}/\text{Fe}]$ ratios from the two stages of ionization are in poor agreement. Literature values for the oscillator strengths for the Sc I lines vary by ~ 0.4 dex (see S92-M5 for discussion) and thus the lines are dropped from this study as well. The only other element in which two stages of ionization are exhibited is Ti, but unfortunately in only two stars, II-85 and IV-47. In these stars, the two $[\text{Ti}/\text{Fe}]$ stages are in rough agreement even though the result is based on only one Ti II line: $[\text{Ti I}/\text{Fe I}]$ and $[\text{Ti II}/\text{Fe II}]$ are 0.30 and 0.14 for

¹⁴This 5 percent correction applies only to Lick Hamilton spectrograph observations made prior to 1995, at which time the optics were upgraded and the 800×800 TI chip was replaced with a 2048×2048 chip. EWs from the upgraded Hamilton are known to be on the system of the Keck I HIRES spectrograph (Shetrone 1996, Johnson 1999.)

IV-47, and 0.18 and 0.24 for II-85. Except for the case of Sc, the agreement between the Lick- and Keck I-based abundances appears therefore to be excellent.

6.1. Re-analysis of Other Lick Observations

In order to expand our analysis to include more M5 abundances of Mg, Al and Eu (observed by us in only 2, 23, and 25 of the 36 stars, respectively), we have sought out EWs in the literature. Fortunately, Shetrone’s (1996) study, based on post-1995 Lick Hamilton spectra, included five M5 stars in common with this study (excluding II-9 which we omitted earlier due to S/N considerations). All of the stars in common are also part of our Lick sample.

In Table 7, we present the results of applying our new models (the right hand columns of Table 2) to the EWs of Shetrone (1996) for Mg, Al, and Eu for the 5 stars in common with our study. For Mg, we consider only the atomic lines, neglecting the results from the MgH features. The averages and standard deviations of the results using the Keck data taken of the two stars for which we are able to derive Mg and Al abundances are also shown. Since both sets of M5 results are within $1\text{-}\sigma$, in subsequent figures we will treat the elemental abundances derived using data we acquired with equal weight to those derived from our re-analysis of the Shetrone (1996) EWs.

Finally in Table 8 we present the mean values of the [el/Fe]-ratios for AGB, RGB, and RGB plus “tip” stars, averaged over the Keck and Lick observations, plus “grand” mean values averaged over all 35 stars (the means exclude II-9 as discussed in §6) taken together.

In Figure 8 we present a “boxplot” to summarize the mean and scatter of each element we analysed in M5. The Keck and Lick results are both represented and the Mg, Al, and Eu abundances include the results obtained by putting the Shetrone (1996) EWs on to our system. This boxplot illustrates the median, data spread, skew, and distribution of the range of values we derived for each of the elements from our program stars, as well as possible outliers. As can be seen in the figure, the abundance range for elements sensitive to proton-capture nucleosynthesis is large whereas the star-to-star abundance variations for all of the heavier elements is quite small, and consistent with the normal scatter resulting from observational error.

7. Relationships among [O/Fe], [Na/Fe], [Al/Fe], and CN Band Strengths

7.1. The Distributions of [O/Fe] and [Na/Fe] with Respect to Evolutionary State

In Figure 9 we plot [Na/Fe] versus [O/Fe] and in Figure 10, [Al/Fe] versus [Na/Fe]. The results are consistent with the expected anti-correlation of Na with O and the correlation of Al with Na (see reviews cited in §1). The shape of these relationships generally follows that seen earlier in M15 (Snedden *et al.* 1997), M10 (Kraft *et al.* 1995), M3 (Kraft *et al.* 1992), M92 (Snedden *et al.* 1991,

Shetrone 1996) and M13 (Shetrone 1996, Kraft *et al.* 1997, Cavallo & Nagar 2000). The ranges of O and Na in M5 are comparable with the large range seen in M13, although the range of Al is distinctly smaller, more in keeping with the other clusters cited. On the other hand the range in O and Al is larger than is found in M4, a cluster with metallicity similar to M5, although the range in Na is about the same (I99-M4).

One star that stands well off the relationships shown in these two figures is I-20, the coolest of the AGB stars in our sample. It has an unusually low Fe II abundance, a fairly low Fe I abundance and by far the largest microturbulent velocity. The low Fe abundances, however, cannot alone account for the high [O/Fe] and [Na/Fe] values, while simultaneously yielding an [Al/Fe] ratio that is too low for its [O/Fe]. Possibly the star is an unresolved binary, consisting of a pair of RGB stars, but this would require that the two components differ substantially in V , since the combined light is only 0.2 mag above the RGB. In that case, the line profiles might indeed be widened, thus accounting for the large v_t value, but would also be unsymmetrical, contrary to their actual appearance. However, I-20 does exhibit the largest H- α emission among our sample for which H- α was recorded on the chip. We note that if I-20 is a pair of RGB stars disguised as an AGB, the $\log g$ for these stars (~ 1.65) would lead to a *further reduction* of 0.1 dex in the [V/Fe]-ratio (see Table 3). At the moment we conclude that I-20 has elevated O and Na abundances compared with other M5 stars, exhibiting in exaggerated form the excess O and Na abundances found previously in IV-59 (Kraft *et al.* 1992, Briley & Smith 1993, Smith *et al.* 1997). The additional anomalous stars noted in Figure 9 are discussed further in §7.2.

When a large sample of M13 giants is divided at $\log g = 1.02$, there is a clear shift of Mg, Na, and O abundances in support of the evolutionary scenario (Kraft *et al.* 1997, Hanson *et al.* 1998). If the present sample of M5 RGB and “tip” stars is divided by evolutionary state, do we find a similar shift that supports the evolutionary picture? In response to this inquiry, we explored the distributions of [O/Fe] and [Na/Fe] when the RGB plus “tip” giants are divided into two virtually equal evolutionary groups: 14 giants having $\log g \leq 1.02$ and 13 having $\log g > 1.02$. The results are shown in histogram form in Figure 11. We performed a Mann-Whitney U-Test (equivalent to a Wilcoxon Rank-Sum Test) to test the hypothesis that the two samples have the same mean of oxygen abundance ratio distribution against the hypothesis that they differ. There is a less than 1% probability that the two samples have the same mean of distribution. Thus we confirm statistically what can be discerned by eye: the two samples have significantly different means of distribution. In contrast with M13, the distributions above and below evolutionary $\log g$ of 1.02 are differently skewed, but in a sense opposite to that expected in the evolutionary scenario. This result, although not incompatible with the primordial scenario, does not rule out the notion that the required evolutionary change could have taken place among giants fainter than those probed by our sample.

7.2. Relationship of CN Band Strengths to [O/Fe] and [Na/Fe]

Measurements of CN band strengths in a substantial number of M5 RGB and AGB stars have been carried out by Smith & Norris (1983, 1993) and by Briley & Smith (1993). Like many other globular clusters, M5 giants present a bimodal distribution of CN band strengths. Smith *et al.* (1997) found that strong CN bands among M5 giants are generally driven by a high abundance of N, and that the index S(3839), which is a measure of the flux in the $\lambda 3883 \text{ \AA}$ CN molecular band relative to that in a nearby comparison region, is anti-correlated with [O/Fe] and correlated with [Na/Fe]. For a scenario in which the star-to-star abundance variations seen here are a result of proton-capture nucleosynthesis, such a behavior of CN band strengths is expected, since C will likely have been processed to N when O is transmuted to N and Ne to Na (Langer *et al.* 1993, Cavallo *et al.* 1998).

The giants studied here add further weight to this picture. In Figure 12, we plot [Na/Fe] and [O/Fe] as a function of the CN bandstrength index $\delta S(3839)$ for 30 giants. The S(3839) values were taken from Smith & Norris (1993), supplemented by Smith & Norris (1983), Briley & Smith (1993) and Smith *et al.* (1997). Where available, the Smith & Norris (1993) values were adopted. In the case of multiple measurements from the other sources, an average value was adopted, subsequent to employing the transformations described in Smith *et al.* (1997). The “raw” S(3839) values are shown in Table 1. Because some of the CN bandstrength measured by S(3839) is sensitive to temperature (given the same C and N abundances, cooler stars have intrinsically larger S(3839) indices than their hotter counterparts), we “detrended” the raw S(3839) index. We fitted a “baseline” as a function of T_{eff} to the S(3839) results, and formed a differential CN strength index,

$$\delta S(3839) = S(3839) - (0.991 - 1.95 \times 10^{-4} \times T_{\text{eff}}).$$

We further binned the stars into “CN-strong” and “CN-weak” groups using Smith & Norris (1993) as a guide, with the exception that we designated the Smith & Norris “intermediate” strength stars, and other stars with similar $\delta S(3839)$ measures, as CN-strong.

We find the $\delta S(3839)$ index to be correlated with Na and anti-correlated with O, as shown in Figure 12. Returning to Figure 9, where we note the stars as being CN-strong (s) or CN-weak (w), we see that the CN-strong stars lie in the low O, high Na part of the diagram, with CN-weak stars dominating the high O, low Na portion. As seen in previous studies of other globular clusters, the Na and O abundance patterns also correlate with the CN strength as inferred by the $\delta S(3839)$ index. A few stars plotted in Figure 9 remain anomalous; we have already noted I-20 and IV-59. The two stars I-68 and III-78 appear to be a bit oxygen-rich for their sodium abundances. II-85 has high [O/Fe] but only an intermediate value of $\delta S(3839)$. I-55 has diminished oxygen and enhanced sodium, opposite to what would be expected from its CN bandstrength index. For this star, the abundances of the two pairs of Na lines have a standard deviation of 0.06 dex and the two oxygen line syntheses are in excellent agreement. However, there is some ambiguity about its CN bandstrength classification: Smith & Norris (1993) give a small S(3839) value, corresponding to that of a CN-weak star but list I-55 as a CN-strong star. We suggest that a closer examination

of the CN measurements of this particular AGB star is required to resolve the ambiguity. The star III-96 appears to have an excessive Na abundance, but the values of $[\text{Na}/\text{Fe}]$ derived from the $\lambda\lambda 5682, 5688 \text{ \AA}$ pair and the $\lambda\lambda 6154, 6161 \text{ \AA}$ pair are in poor agreement.

Similar correlations between CN-strength and location in the Al-Na correlation are found in Figure 10, where we find, in general, that the CN-strong stars lie in the high Al, high Na part of the diagram. But again there are a few anomalous stars like I-20 and I-55. We conclude that, within the errors of our abundance determinations, most M5 giants follow the expected pattern of proton-capture nucleosynthesis with only a few exceptions, but these exceptions are compatible with the existence of primordial abundance variations among at least a few members of M5.

Figure 12 also demonstrates that within both the CN-weak and CN-strong groups there is an intrinsic spread in $\delta S(3839)$, $[\text{O}/\text{Fe}]$, and $[\text{Na}/\text{Fe}]$. Even the CN-weak stars themselves show an intrinsic dispersion in $\delta S(3839)$, $[\text{O}/\text{Fe}]$, and $[\text{Na}/\text{Fe}]$. The same is true for the CN-strong stars. If these observations are not a result of scatter due to observational error, then they are consistent with a “primordial” scatter of Na and O, produced by proton-capture nucleosynthesis in an earlier generation of stars, which has subsequently been modified by deep mixing in the sample stars themselves.

8. A Comparison of $[\text{el}/\text{Fe}]$ Ratios in M4 and M5

Although many clusters have giants with variations in C, N, O, Na, Al, and Mg that are attributable to the proton-capture process, they also usually yield $[\text{el}/\text{Fe}]$ ratios of the Fe-peak elements, α -capture elements such as Si, Ca, and Ti and heavy neutron-capture elements such as Ba and Eu that are stable and “normal” with respect to typical halo field stars. In this respect, M5 is no exception. In Table 9 we list $[\text{el}/\text{Fe}]$ ratios for M5 together with the mean of a large sample of halo field subdwarfs at $[\text{Fe}/\text{H}] \simeq -1.2$ (Fulbright 2000, 2001), for most of the elements, supplemented by field giants (Gratton & Sneden 1994) in the case of La. In the upper part of this table, we consider only those elements not subject to proton-capture nucleosynthesis. Among these elements, the agreement between M5 and the halo field subdwarfs is good, the difference never exceeding $1\text{-}\sigma$ (for M5). In the lower part of this table we add rows for $[\text{Na}/\text{Fe}]$ and $[\text{Al}/\text{Fe}]$. In contrast to cluster stars, field stars do not show evidence for enhanced Na and Al as a result of proton captures on Ne and Mg, respectively (Hanson *et al.* 1998, Kraft 1999, Gratton *et al.* 2000), so it is not surprising that M5 giants on the average show higher $[\text{Na}/\text{Fe}]$ and $[\text{Al}/\text{Fe}]$ values than are found in halo field subdwarfs.

We wish to compare $[\text{el}/\text{Fe}]$ -ratios in M5 with M4, a cluster having nearly the same metallicity as M5. However, the M5 $[\text{el}/\text{Fe}]$ ratios listed in Table 9 come from the revised method of this paper. The abundances in M4 had been derived assuming that $\log g$ could be set from the ionization equilibrium of Fe I and Fe II. Unfortunately, for the M4 stars we cannot set $\log g$ from the Alonso *et al.* (1999) relation between $(B - V)$ and T_{eff} plus application of stellar evolution. M4 is heavily

and differentially reddened, and the ratio of total to selective absorption $R_V = A_V/E(B - V)$ is not the normal value of 3.2, but is estimated to lie in the range 3.1 to 4.0 (Dixon & Longmore 1993; I99-M4). Thus A_V is not accurately known.

To gain an idea of the effect on [el/Fe] ratios in M4 if we were to adopt the same approach consistent with the non-LTE precepts of TI99, we turn the problem around: we adopt the geometrical distance (1.7 kpc) given by Peterson *et al.* (1995) and increase the traditionally derived values of $\log g$ by an amount that offsets [Fe/H] from Fe I and Fe II by the same amount as we have derived for M5, *i.e.*, 0.09 dex. From Table 2 of I99-M4, we find that the values of $\log g$ of giants in M4 need to be increased by 0.12 dex. Again from Table 3 we see that the effect of this increase on [el/Fe]-ratios is actually quite small: for O, Na, Mg, Al, Si, Ca, Sc, Ti, La, and Eu, the corrections do not exceed 0.02 dex. The reduction in [Ba/Fe] is a bit larger: 0.04 dex. These values, therefore slightly revised from those given in Table 5 of I99-M4, are listed in the last column of Table 9. We conclude that any comparison of [el/Fe] ratios between these two clusters is nearly independent of the analysis technique. But two consequences of the revised approach are noteworthy. First, for M4, $\langle [\text{Fe}/\text{H}] \rangle = -1.17$ and -1.08 if derived from Fe I and Fe II, respectively. Second, for a geometrical distance of 1.7 kpc and the revised values of $\log g$, we obtain a ratio of total to selective absorption $R_V = 3.9$ (§3.4 of I99-M4) if $\langle E(B - V) \rangle = 0.37$ (Dixon & Longmore 1993).

To put the I99-M4 results on the M5 system of analysis used in this study, we have applied the $\delta[\text{el}/\text{Fe}]$ corresponding to the 0.12 dex increase in $\log g$. Most of the mean values of [el/Fe] listed in Table 9 for M4 and M5 are derived from 24 and 35 stars respectively, and therefore the standard deviations are generally quite small. In addition, systematic errors are likely not to be a problem since the methods of analysis are basically the same. Among most Fe-peak and α -element abundances, the agreement between M4 and M5 is good, generally within $1\text{-}\sigma$. The main exception seems to be [Si/Fe]: the Si abundance in M4 exceeds that of M5 by about $3\text{-}\sigma$. Similar $3\text{-}\sigma$ overabundances in M4 compared with M5 (and the field) are found in Ba and La. Al is also higher in M4 than in M5 (and the field), but the significance of this result is less clear since Al is a product of proton-capture nucleosynthesis and known to be highly variable among cluster stars.

Based on our large stellar sample and the updated I99-M4 results, we extend the work of I99-M4 and confirm what Brown & Wallerstein (1992) found from a small sample of M4 stars: Si, Al, Ba and La abundances are unusually large in M4. We confirm also the earlier study of S92-M5 which showed that M5 has “normal” abundances. In the comparison of M5 with M4, we did not find the difference in Mg reported by I99-M4 but, in our observations, the Mg I lines were recorded in the spectra of only two M5 giants. The mean abundance for our two stars is 0.39 ± 0.03 ($\sigma = 0.07$) which is comparable to the mean in I99-M4, 0.42 ± 0.02 ($\sigma = 0.08$). In the I99-M4 study, the difference reported with respect to M5 was determined using the results of Shetrone (1996). Employing Shetrone’s published EWs and the revised models we have derived in this analysis, we obtain an average [Mg/Fe]-ratio of $+0.32 \pm 0.03$ ($\sigma = 0.07$) for the Shetrone data, which, combined with the two stars from our sample, gives an average [Mg/Fe]-ratio of 0.34 ± 0.03 ($\sigma = 0.07$). We find that the difference in Mg between M4 and M5 is a bit more than $1\text{-}\sigma$.

In the following boxplots, we show the range of abundances found in both M4 and M5: Figure 13 illustrates the elements which may be sensitive to proton-capture nucleosynthesis, Figure 14 shows the heavier α - and Fe-peak elements, and Figure 15 illustrates the s - and r -process element abundances. In these plots, it is apparent that the Al “floor” in M4 is elevated, while the range of Al abundances is roughly equal to that of M5; Si is elevated; and both Ba and La are elevated. The other elements show sufficient overlap to be consistent with showing no significant differences in the abundance ratios. Could the enhanced Ba and La abundances in M4 found by Brown & Wallerstein (1992) and I99-M4 be simply due to the weighting of the AGB stars in their samples? First, we point out that not a single star in M5 (AGB, RGB or “tip”) has been found to possess a La abundance that is as large as even the lowest value found in M4. Next, we note that in the I99-M4 study, the mean Ba and La abundances for the AGB stars (as determined using their Figure 12) are the same as those in the rest of the sample. Since the Ba and La enhancements in M4 are not a result of slow neutron-capture synthesis occurring in the stars themselves, they must be signatures of primordial enrichments of the material out of which the M4 stars formed.

9. Comparisons with Other Clusters

In Figure 16, we plot $[\text{Na}/\text{Fe}]$ versus $[\text{O}/\text{Fe}]$ values for M4 and M5 and globular clusters that bracket M4 and M5 in metallicity. The plot illustrates a difference in abundance patterns that can be divided into two groups. The O versus Na anti-correlation found in M5 resembles that found in the slightly more metal-poor clusters M3, M10 and M13 ($\langle[\text{Fe}/\text{H}]\rangle \sim -1.5$ to -1.6). The pattern is quite different from that found in M4. Instead, M4’s behavior seems to be much more like that of M71, a disk cluster of much higher metallicity ($\langle[\text{Fe}/\text{H}]\rangle \sim -0.8$; Sneden *et al.* 1994). We note that these clusters can also be binned by horizontal branch morphology. According to the catalog compiled by Harris (1996; June 22, 1999 revision), M3, M5, M10, and M13 all have $(B - R)(B + V + R) > 0$ (where B , V , and R represent the number of stars on the blue end of the HB, in the Hertzsprung gap, and on the red end, respectively) whereas M4 and M71 have $(B - R)(B + V + R) < 0$. In addition, Shetrone & Keane (2000) note that the Na-O and Al-O anticorrelations between the slightly more metal-poor clusters NGC 288 ($\langle[\text{Fe}/\text{H}]\rangle = -1.39$) and NGC 362 ($\langle[\text{Fe}/\text{H}]\rangle = -1.33$) resemble those of M4 (I99-M4) and M5 (S92-M5), respectively.

The important conclusion established by this investigation is that there is no definitive “single” value of $[\text{el}/\text{Fe}]$ at a given $[\text{Fe}/\text{H}]$ for at least some α -capture, odd- Z , and s -process elements, in this case, Si, Al, Ba and La. It is therefore not clear that one can claim some “exact” value of (say) $[\text{Si}/\text{Fe}]$ that characterizes globular cluster or halo field stars at a given $[\text{Fe}/\text{H}]$. Rather, there is a spread that is certainly real and not a result simply of observational or analytical error. Our result is therefore consistent with an increasingly large body of evidence (*e.g.*, Sneden 2000) that in the halo $[\text{el}/\text{Fe}]$ ratios are not universal at a given metallicity. For example, the outer halo clusters Rup 106 and Pal 12 have very low (close to solar) α -capture element abundances (Brown *et al.* 1997) as do a few subdwarfs having unusually large absolute angular momenta (Carney 1999, Fulbright 2001, and

references therein). Very high Si abundances ($\langle[\text{Si}/\text{Fe}]\rangle \sim 0.6$) are observed in the very metal-poor ($\langle[\text{Fe}/\text{H}]\rangle \sim -2.4$) globular cluster M15 (Sneden *et al.* 1997). The overabundance of Ba in M15 compared with M92, two clusters of very similar metallicity, is well established (Sneden *et al.* 2000). It has also been known for some time that Ba and other *s*-process species are greatly enhanced in metal-rich giants of ω Cen compared with field halo and globular cluster stars of comparable metallicity (Vanture *et al.* 1994; Norris & Da Costa 1995). In fact, there exists in ω Cen a stellar sample which possesses nearly identical elemental overabundances of $[\text{Si}/\text{Fe}]$, $[\text{Al}/\text{Fe}]$, and $[\text{Ba}/\text{Fe}]$ as seen in M4. However, in ω Cen, the sample consists of stars possessing a range of metallicities ($-0.5 < [\text{Fe}/\text{H}] < -2.0$). Even more striking is the Eu deficiency found among ω Cen giants of intermediate metallicity (Smith *et al.* 2000).

10. Summary and Conclusions

We have analysed the chemical abundances of 36 M5 giant stars by two different techniques. We employed “traditional” spectroscopic analysis procedures, setting T_{eff} by satisfying the constraint of iron excitation potential equilibrium, setting v_t by satisfying the constraint of iron equivalent width equilibrium, setting $\log g$ by satisfying the constraint of iron ionization equilibrium, and satisfying the additional constraint that the derived $[\text{Fe}/\text{H}]$ does not vary systematically over the range of T_{eff} and $\log g$ represented by the cluster program stars. Satisfying these constraints led to models whose spectroscopic $\log g$ values were ~ 0.5 dex lower than expected, which in turn led to $\langle[\text{Fe}/\text{H}]\rangle$ ratios 0.15 dex lower among our AGB sample than among our RGB sample. These outcomes are consistent with known problems that result from applying LTE assumptions to non-LTE atmospheres.

We investigated a number of alternative approaches to the analysis, seeking to resolve the outcomes without resorting to invoking non-LTE effects. However, regardless of which T_{eff} -scale or $\log g$ -scale we adopted, the $[\text{Fe}/\text{H}]$ based on Fe I remained significantly smaller on the AGB as compared with the RGB and “tip” stars. Accordingly, we adopted an analysis consistent with the non-LTE precepts as discussed by Thévenin & Idiart (1999), employing “new” models with evolutionary values of $\log g$ on the same system as those of previous M5 work. These results yielded $\langle[\text{Fe}/\text{H}]\rangle = -1.21$ ($\sigma = 0.06$), that were neither dependent on T_{eff} nor $\log g$ and are in good agreement with previously derived values for the metallicity of M5 in the literature (*e.g.*, $\langle[\text{Fe}/\text{H}]\rangle = -1.4$, Zinn & West 1984; $\langle[\text{Fe}/\text{H}]\rangle = -1.17$, Sneden *et al.* 1992). Applying the same procedures to the M4 results of Ivans *et al.* (1999), we re-determine the metallicity of M4 to be $\langle[\text{Fe}/\text{H}]\rangle = -1.08$ ($\sigma = 0.02$). The remaining abundances in M4 are offset by an amount equivalent to an increase in $\log g$ of 0.12 dex (see Table 2 of Ivans *et al.* 1999). Applying this increase in $\log g$ to the M4 stars, we derive the ratio of total to selective absorption $R_V = 3.9$ (see §3.4 of Ivans *et al.* 1999).

With the revised method of analysis, we find good agreement between M5 and M4 (and the field) in most of the Fe-peak and α -element abundances. The exception is silicon. The $[\text{Si}/\text{Fe}]$

abundance in M4 exceeds that of M5 by $\sim 3\sigma$. Ba and La are similarly overabundant in M4 with respect to M5 (and the field), as is aluminum. However, since Al is sensitive to proton-capture nucleosynthesis, the range of aluminum abundances in both clusters mask the overall difference in the “floor” abundances. Based on these large stellar samples, we confirm and extend the previous findings for both of these clusters: Si, Al, Ba, and La are enhanced in M4, whereas M5 has “normal” abundances.

In M5, we find the classic anti-correlation of O and Na abundances, and correlated Al and Na abundances. And, the behavior of these abundances is further correlated with the CN strength index, $\delta S(3839)$: stars with larger CN indices also have larger Al abundances, larger Na abundances and lower O abundances than stars with lower CN indices. This behavior is consistent with that seen in previous studies of other globular clusters and follows the expected pattern of proton-capture nucleosynthesis (*i.e.*, low oxygen abundances are usually accompanied by low carbon and enhanced nitrogen abundances. Thus, stronger CN bands, reflecting higher N abundances, belong to stars that are more highly CNO-processed).

We binned the M5 RGB and “tip” giants into two evolutionary groups by $\log g$, and find that the O and Na abundances are different for the two groups: the stars with lower $\log g$ have higher O and lower Na abundances on average than the stars with higher values of $\log g$. Thus, in M5, the dependence of the abundance variations on $\log g$ is in the *opposite* sense to that found in M13 by Kraft *et al.* (1997), where the relationship provided strong evidence in support of the evolutionary scenario. The present analysis of M5 giants does not necessarily rule out the evolutionary scenario, but it neither provides support for it nor is it incompatible with the primordial scenario. In fact, both may be at work. Our observations of the spread in [O/Fe], [Na/Fe], and [Al/Fe] ratios in both the CN-strong and CN-weak groups are consistent with the idea that an earlier generation of stars may have enriched some of the material out of which the current sample formed then, once on the RGB, the stars were subject to deep mixing, further altering the abundances. Thus, deep mixing on the RGB would explain the spreads within the CN-strong and CN-weak groups, and primordial enrichment the difference between the two groups.

In comparison with clusters that bracket M4 and M5 in metallicity, we find that the abundance patterns can be divided into two groups: the O vs Na anti-correlation found in M5 resembles the pattern seen in slightly more metal-poor globular clusters M3, M10, and M13 ($\langle [\text{Fe}/\text{H}] \rangle = -1.5$ to -1.6) whereas the anti-correlation found in M4 resembles that of the more metal-rich disk cluster M71 ($\langle [\text{Fe}/\text{H}] \rangle \sim -0.7$). These similarities extend to the HB morphology of the clusters: according to the catalog compiled by Harris (1996), M3, M5, M10, and M13 all have $(B - R)(B + V + R) > 0$ (where B , V , and R represent the number of stars on the blue end of the HB, in the Hertzsprung gap, and on the red end, respectively) whereas M4 and M71 have $(B - R)(B + V + R) < 0$.

We conclude that there is no “single” value of $[\text{el}/\text{Fe}]$ at a given $[\text{Fe}/\text{H}]$ for at least some α -capture, odd-Z, and s -process elements, in this case, Si, Al, Ba, and La. The spread is real and not a result due to observational or analytical error. Our result is therefore consistent with

an increasingly large body of evidence (*e.g.*, Sneden 2000) that in the halo [el/Fe] ratios are not universal at a given metallicity. The dichotomy between M4 and M5 established here adds more evidence favoring the existence of considerable abundance diversity in the Galactic halo.

We are happy to acknowledge that this research was partially funded by NSF grants AST-9618351 to R.P.K. and G.H.S. and AST-9618364, AST-9987162 to C.S. and has made use of NASA’s Astrophysics Data System Bibliographic Services. We are indebted to Eric Sandquist for supplying the exquisite photometry of M5 as well as for responding to queries regarding individual stars. Andy McWilliam has our gratitude for sending along his most recent calculations of V hfs and for sharing his code and expertise. We thank Kirk Gilmore for sharing with us his $2\mu\text{m}$ image of the cluster. We appreciate Earl Luck’s help in tracking down some of the laboratory log gf -values and Jennifer Johnson’s & Jon Fulbright’s assistance in transporting SPECTRE onto a different platform. John Norris, Gary Da Costa, and George Wallerstein have our appreciation for both taking the time to read a draft of the paper and subsequently offering thoughtful comments and useful suggestions that improved it. Ruth Peterson also has our thanks for helpful discussions regarding Kurucz atmospheres. The anonymous referee’s detailed comments and thoughtful suggestions helped improve the paper and are much appreciated. I.I.I. gratefully acknowledges the financial support of a Continuing Fellowship from the University of Texas at Austin and the Audrey Jorss Commemorative Fellowship from the Australian Federation of University Women Queensland Branch during the time that this work was performed and thanks sincerely the members of the Research School of Astronomy and Astrophysics of the Australian National University at Mount Stromlo Observatory for their hospitality during the preparation of this paper.

REFERENCES

- Allende Prieto, C., García López, R., Lambert, D. L. & Gustafsson, B. 1999, ApJ, 527, 879
- Allende Prieto, C. & Lambert, D. L. L. 2000, AJ, 119, 2445
- Alonso, A., Arribas, S., Martínez-Roger, C. 1999, A&AS, 117, 227
- Alonso, A., Arribas, S., Martínez-Roger, C. 1999, A&AS, 140, 261
- Bates, B., Kemp, S. N. & Montgomery, A. S. 1993, A&AS, 97, 937
- Bell, R. A. & Gustafsson, B. 1978, A&AS, 34, 229
- Blackwell, D. E., Petford, A. D., Arribas, S., Haddock, D. J. & Selby, M. J. 1990, A&A, 232, 396
- Briley, M. M. & Smith, G.S. 1993, PASP, 105, 1260
- Briley, M. M., Bell, R. A., Hesser, J. E. & Smith, G. H. 1994, Can. J. Phys., 72, 772
- Briley, M., Smith, V. V., Suntzeff, N. B., Lambert, D. L., Bell, R. A. & Hesser, J. E. 1995, Nature, 383, 604

- Brown, J. A. & Wallerstein 1992, *AJ*, 104, 1818
- Brown, J. A., Wallerstein, G. & Zucker, D. 1997, *AJ*, 114, 180
- Buonanno, R., Corsi, C. E., Fusi Pecci, F. 1981, *MNRAS*, 196, 435
- Carney, B. W. 1999, in *The Third Stromlo Symposium: The Galactic Halo*, ed. B. K. Gibson, T. S. Axelrod, & M. E. Putnam, *ASP Conf. Ser.* 165, 230
- Carretta, E. & Gratton, R. G. 1997, *A&AS*, 121, 95
- Cavallo, R.M. & Nagar, N. M. 2000, *AJ*, 120, 1364
- Cudworth, K. M. 1979, *AJ*, 84, 1866
- Cudworth, K. M. & Hanson, R. B. 1993, *AJ*, 105, 168
- Da Costa, G. S. 1997, in *Fundamental Stellar Properties: The Interactions Between Observations and Theory*, ed. T. R. Bedding, A. J. Booth & J. Davis, *IAU Symp.* 189, 193
- Denissenkov, P. A., Da Costa, G. S., Norris, J. E. & Weiss, A. 1998, *A&A*, 333, 926
- Djorgovski, S. 1993, in *Structure and Dynamics of Globular Clusters*, ed. S. G. Djorgovski & G. Meylan, *ASP Conf. Ser.* 50, 373
- Dumont, S., Heidman, N., Jeffries, J. T. & Pecker, J.-C. 1975, *A&A*, 40, 127
- ESA, 1997, *The Hipparcos and Tycho Catalogues* (ESA SP-1200; Noordwijk: ESA)
- Fitzpatrick, M. J. & Sneden, C. 1987, *BAAS*, 19, 1129
- Frogel, J. A., Persson, S. E., & Cohen, J. G. 1983, *ApJS*, 53, 713
- Fuhr, J. R., Martin, G. A. & Weise, W. L. 1988, *J. Phys. Chem. Ref. Data*, 17, Suppl. No. 4, 1
- Fuhrmann, K., Pfeiffer, M., Frank, C., Reetz, J. & Gehren, T. 1997, *A&A*, 323, 909
- Fulbright, J. 2000, *AJ*, 120, 1841
- Fulbright, J. 2001, *AJ*, Submitted
- Fulbright, J. P. & Kraft, R. P. 1999, *AJ*, 118, 527
- Gratton, R. G. & Sneden, C. 1991, *A&A*, 241, 501
- Gratton, R. G. & Sneden, C. 1994, *A&A*, 287, 927
- Gratton, R. G., Fusi Pecci, F., Carretta, E., Clementini, G., Corsi, C. E., & Lattanzi, M. 1997, *ApJ*, 491, 749.

- Gratton, R. G., Sneden, C., Carretta, E. & Bragaglia, A. 2000, *A&A*, 354, 169
- Gratton, R. G., Bonifacio, P., Bragaglia, A., Carretta, E., Castellani, V., Centurion, M., Chieffi, A., Claudi, R., Clementini, G., D'Antona, F., Desidera, S., Francois, P., Grundahl, F., Lucatello, S., Molaro, P., Pasquini, L., Sneden, C., Spite, F., & Straniero, O. 2001, *A&A*, 369, 87
- Gustafsson, B., Bell, R. A., Ericksson, K. & Nordlund, A. 1975, *A&A*, 42, 407
- Hanson, R. B., Sneden, C., Kraft, R. P. & Fulbright, J. 1998, *AJ*, 116, 1286
- Harris, W. E. 1996, *AJ*, 112, 1487
- Hearnshaw, J. B. 1976, *A&A*, 51, 71
- Houdashelt, M. L., Bell, R. A. & Sweigart, A. V. 2000, *AJ*, 119, 1448
- Ivans, I. I., Sneden, C., Kraft, R. P., Suntzeff, N. B., Smith, V. V., Langer, G. E. & Fulbright, J. P. 1999, *AJ*, 118, 1273 (I99-M4)
- Johnson, J. 1999, Ph.D. thesis, Univ. California, Santa Cruz
- Jones, R. V., Carney, B. W. & Latham, D. W. 1988, *ApJ*, 332, 206
- Kovtykh, V. V. & Andrievsky, S. M. 1999, *A&A*, 351, 597
- Kraft, R. P. 1994, *PASP*, 106, 553
- Kraft, R. P. 1999, *Ap&SS*, 265, 153
- Kraft, R. P. 2001, in *Highlights of Astronomy*, ed. H. Rickman (A.S.P., Provo, Utah), Vol. 12, in press
- Kraft, R. P., Sneden, C., Langer, G. E. & Prosser, C. F. 1992, *AJ*, 104, 645
- Kraft, R. P., Sneden, C., Langer, G. E., Shetrone, M. D., & Bolte, M. 1995, *AJ*, 109, 2586
- Kraft, R. P., Sneden, C., Smith, G. H., Shetrone, M. D., Langer, G. E., & Pilachowski, C. A. 1997, *AJ*, 113, 279
- Lambert, D. L., Heath, J. E., Lemke, M. & Drake, J. 1996, *ApJS*, 103, 183
- Lawler, J. E., Bonvallet, G. & Sneden, C. 2001, *ApJ*, Submitted
- Layden, A. C., Hanson, R. B., Hawley, S. L., Klemola, A. R. & Hanley, C. J. 1996, *AJ*, 112, 2110
- Luck, R. E. & Lambert D. L. 1985, *ApJ*, 298, 782
- Luck, R. E., Moffett, T. J., Barnes, T. G., III & Gieren, W. P. 1998, *AJ*, 115, 605

- Martin, W. C., Fuhr, J. R., Kelleher, D. E., Musgrove, A., Sugar, J., Wiese, W. L., Mohr, P. J. & Olsen, K. (1999) NIST Atomic Spectra Database (version 2.0). Available: <http://physics.nist.gov/asd> [1999 March 22]. National Institute of Standards and Technology, Gaithersburg, MD.
- McWilliam, A., 1997, *ARA&A*, 35, 503
- McWilliam, A., 1998, *AJ*, 115, 1640
- McWilliam, A. & Rich, R. M. 1994, *ApJS*, 91, 749
- McWilliam, A., Preston, G. W., Sneden, C. & Searle, L. 1995, *AJ*, 109, 2757
- Norris, J. E. & Da Costa, G. S. 1995, *ApJ*, 441, 81
- Pilachowski, C. A., Sneden, C. & Kraft, R. P., 1996, *AJ*, 111, 1689 (1996a)
- Pilachowski, C. A., Sneden, C. Kraft, R. P., Langer, G. E. 1996, *AJ*, 112, 545 (1996b)
- Rees, R. F., Jr. 1993, *AJ*, 106, 1524
- Reid, I. N. 1997, *AJ*, 114, 161
- Ryan, S. G., Norris, J. E. & Beers, T. C. 1996, *ApJ*, 471, 254
- Sandage, A. & Cacciari, C. 1990, *ApJ*, 350, 645
- Sandquist, E. L., Bolte, M., Stetson, P. B., Hesser, J. E. 1996, *ApJ*, 470, 910
- Schnabel, R., Kock, M. & Holweger, H. 1999, *A&A*, 342, 610
- Sekiguchi, M. & Fukugita, M. 2000, *AJ*, 120, 1072
- Shetrone, M. D. 1996, *AJ*, 112, 2639
- Shetrone, M. D. & Keane, M. J. 2000, *AJ*, 119, 840
- Smith, G. H. & Norris, J. E. 1983, *ApJ*, 264, 215
- Smith, G. H. & Norris, J. E. 1993, *AJ*, 105, 173
- Smith, G. H., Shetrone, M. D., Briley, M. M., Churchill, C. W. & Bell, R. A. 1997, *PASP*, 109, 236
- Smith, V. V., Suntzeff, N. B., Cunha, K., Gallino, R., Busso, M., Lambert, D. L. & Straniero, O. 2000, *AJ*, 119, 1239
- Sneden, C. 1973, *ApJ*, 184, 839
- Sneden, C. 1999, *Ap&SS*, 265, 145

- Sneden, C. 2000, in 35th Liege Int. Ap. Coll., The Galactic Halo, from Globular Clusters to Field Stars, ed. A. Noels, P. Magain, D. Caro, E. Jehin, G. Parmentier, & A. Thoul (Liège Belgium: Institut d’Astrophysique et de Géophysique), p. 159
- Sneden, C., Kraft, R. P., Prosser, C. F. & Langer, G. E. 1991, *AJ*, 102, 2001
- Sneden, C., Kraft, R. P., Prosser, C. F. & Langer, G. E. 1992, *AJ*, 104, 2121 (S92-M5)
- Sneden, C., Kraft, R. P., Langer, G. E., Prosser, C. F. & Shetrone, M. D. 1994, *AJ*, 107, 1773
- Sneden, C., Kraft, R. P., Shetrone, M. D., Smith, G. H., Langer, G. E., & Prosser, C. F. 1997, *AJ*, 114, 1964
- Sneden, C., Pilachowski, C. A. & Kraft, R. P. 2000, *AJ*, 120, 1351
- Suntzeff, N. B. 1993, in The Globular Cluster-Galaxy Connection, ed. G. H. Smith & J. B. Brodie, ASP Conf. Ser. 48, 167
- Thévenin, F. 1990, *A&A*, 82, 179
- Thévenin, F. & Idiart, T. P. 1999, *ApJ*, 521, 753 (TI99)
- Vanture, A. D., Wallerstein, G. & Brown, J. A. 1994, *PASP*, 106, 835
- Vogt, S. S. 1987, *PASP*, 99, 1214
- Vogt, S. S., Allen, S. L., Bigelow, B. C., Bresee, L., Brown, B., Cantrall, T., Conrad, A., Couture, M., Delaney, C., Epps, H. W., Hilyard, D., Hilyard, D. F., Horn, E., Jern, N., Kanto, D., Keane, M. J., Kibrick, R. I., Lewis, J. W., Osborne, J., Pardeilhan, G. H., Pfister, T., Ricketts, T., Robinson, L. B., Stover, R. J., Tucker, D., Ward, J. & Wei, M. Z. 1994, *SPIE*, 2198, 362
- Wallerstein, G. 1962, *ApJS*, 6, 407
- Wallerstein, G, Iben, I. Jr., Parker, P., Boesgaard, A. M., Hale, G. M., Champagne, A. E., Barnes, C. A., Käppeler, F., Smith, V. V., Hoffman, R. D., Timmes, F. X., Sneden, C., Boyd, R. N., Meyer, B. S., & Lambert, D. L. 1997, *Rev. Mod. Phys.*, 69, 995
- Zinn, R. & West, M. J. 1984, *ApJS*, 55, 45

Appendix

Table 10 shows the atomic parameters of the lines used in this study, adopting the linelist employed in Ivans *et al.* (1999; “I99-M4”). Most of the lines used in the I99-M4 study are the same as those used in earlier papers of the Lick-Texas group. In I99-M4, however, the metallicity of M4 metallicity forced a culling of many blended lines which left a list of only fairly strong lines (see I99-M4 for details). Ivans *et al.* then added to the list clean Fe lines of low to medium strength as well as additional other elemental lines for which laboratory values of the atomic parameters were available from other M4 studies. Also added to the I99-M4 linelist were three La lines for which astrophysical gf -values had been derived by the inverse solar method by Brown & Wallerstein (1992). However, one of these La lines ($\lambda 6390 \text{ \AA}$) now has an up-to-date laboratory gf -value determination (Lawler *et al.* 2001) which we employed here as well as in the updated I99-M4 results. By maintaining the same linelists in both studies, we are able to compare the results of M4 and M5 directly.

Table 11 illustrates the abundances derived from a traditional spectroscopic analysis as outlined in §3.1. These should be compared with mean values from Table 5. For specific species, we examine the “split” between RGB and AGB $\langle [el/Fe] \rangle$ ratios, based on the “new” vs “traditional” analysis.

1. Oxygen: $\langle [O/Fe] \rangle$ shows the same split of 0.06 dex between the RGB and AGB in both the “new” and “traditional” analyses but the scatter is large because of the Na versus O anti-correlation (see §5 and S92-M5).
2. Sodium and aluminum: there is a large scatter but, as with O, shows no significant difference in mean values between RGB and AGB. The scatter probably reflects true star-to-star abundance differences.
3. Silicon: $\langle [Si/Fe] \rangle$ is increased by 0.01 dex over the “traditional” value. However, the split between the RGB and AGB stays the same.
4. Calcium: the split in $\langle [Ca/Fe] \rangle$ between the RGB and AGB remains the same; there is only a slight change in $\langle [Ca/Fe] \rangle$ overall.
5. Titanium: the difference in $\langle [Ti/Fe] \rangle$ between the AGB and RGB is somewhat reduced in the “new” analysis.
6. Vanadium: in the “traditional” analysis $\langle [V/Fe] \rangle = -0.12$, taken over all stars, but $\langle [V/Fe] \rangle$ is more negative by 0.17 dex on the AGB compared with its value on the RGB. The “new” analysis produces a smaller difference of 0.09 dex, and a slightly more positive overall mean of -0.10 .
7. Manganese: The “new” analysis reduces the split between the branches by 0.03 dex while the overall mean was reduced by 0.02 dex.
8. Nickel: The “new” and “traditional” values of $\langle [Ni/Fe] \rangle$ are both -0.05 , and the two branches are in very close agreement in both cases.

9. Heavy elements: The difference in $\langle[\text{el}/\text{Fe}]\rangle$ between the two branches in the “new” analysis is reduced for Ba (by 0.05 dex), La (by 0.04 dex) and Eu (by 0.04 dex), as compared to the “traditional” analysis.

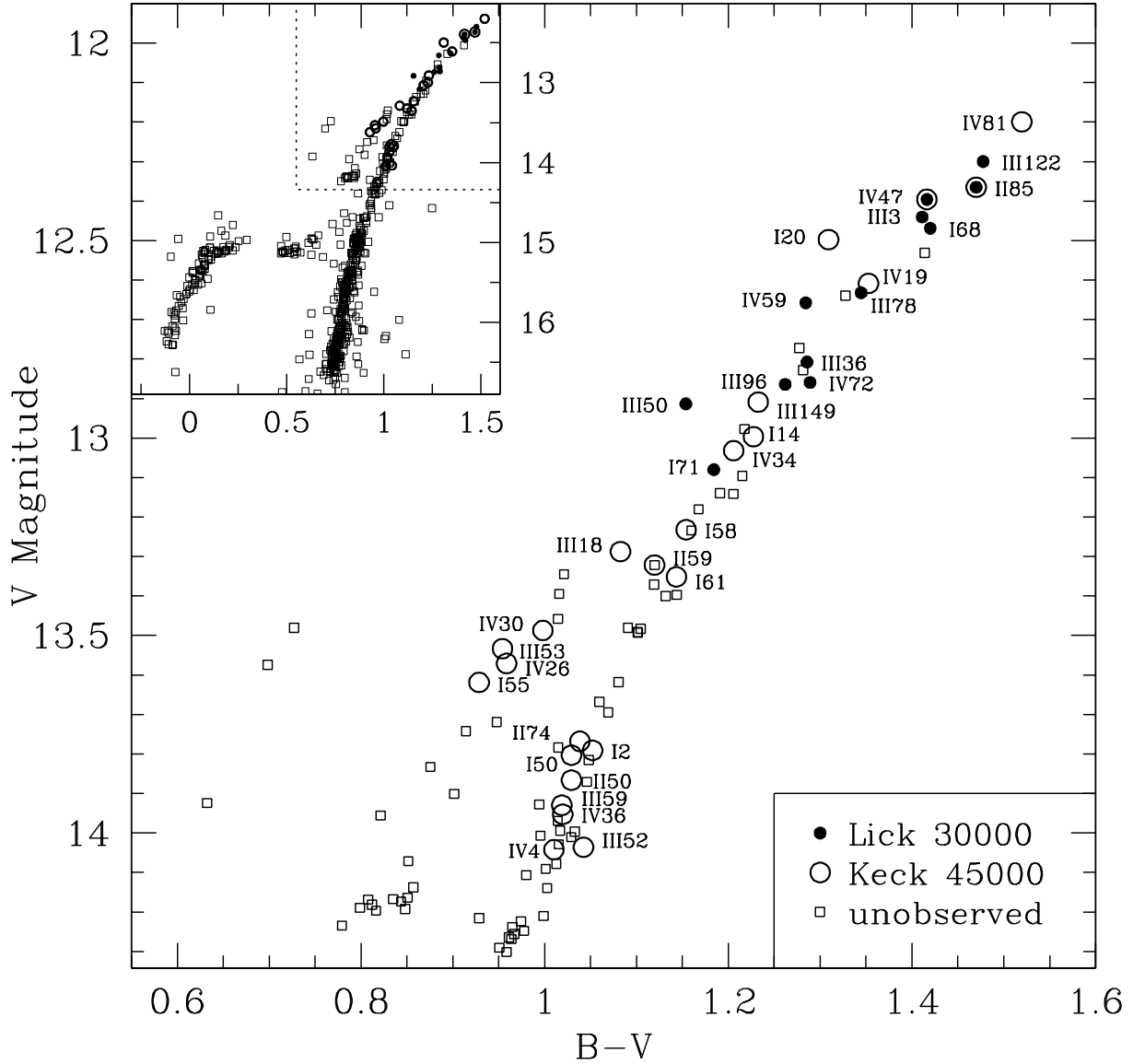


Fig. 1.— CMD of M5 with photometry from Sandquist *et al.* (1996; 2000, private communication), showing the positions of our program stars on the AGB and RGB. The symbols are given in the figure legend and correspond to the observatory and resolution used for each observation. The inset diagram shows the program stars plotted in relation to all Sandquist *et al.* stars of magnitude ≤ 16.9 .

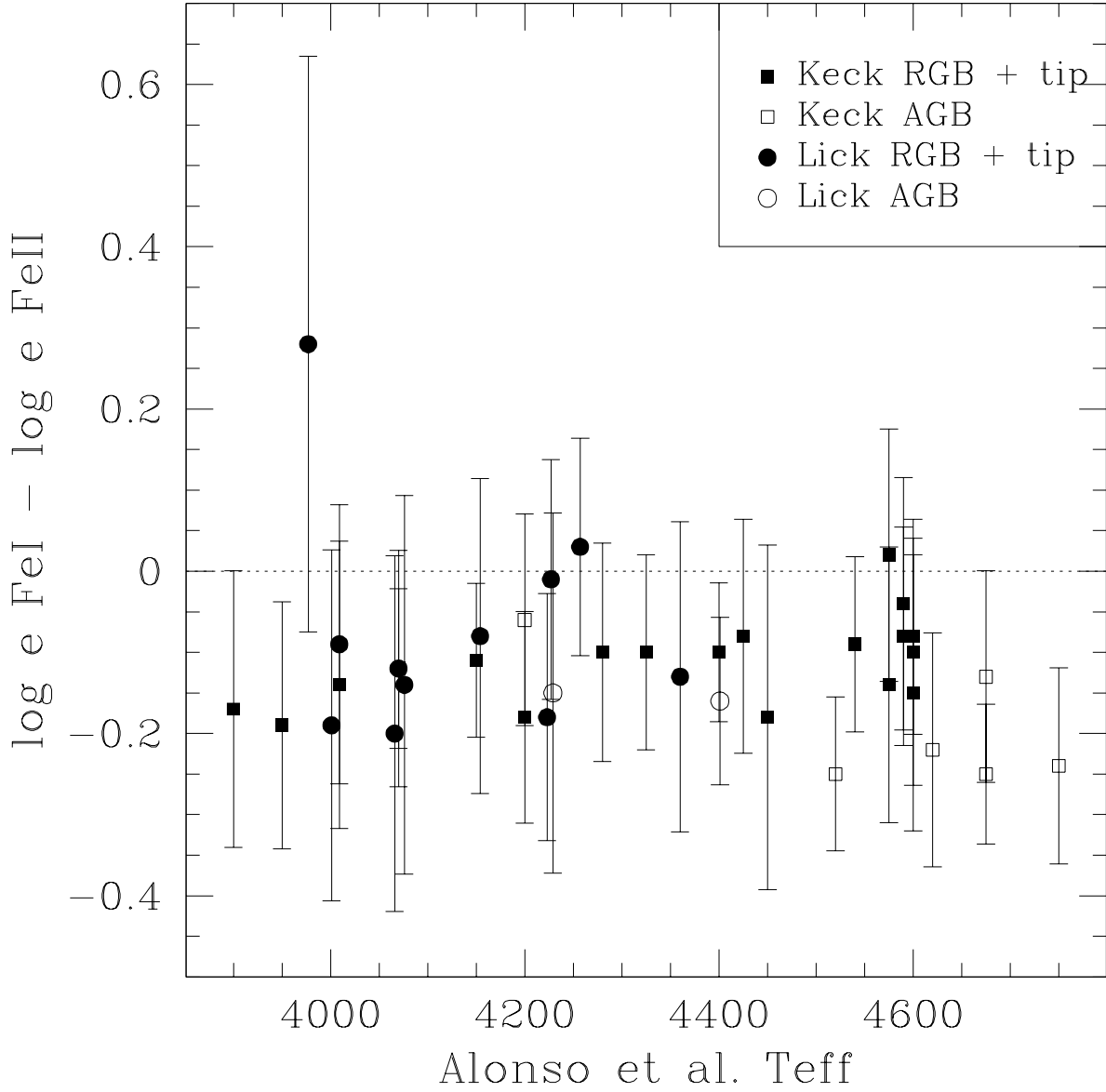


Fig. 2.— $\log \epsilon (\text{Fe I})$ minus $\log \epsilon (\text{Fe II})$ as a function of T_{eff} (as derived from the calibration of Alonso *et al.* 1999) for our M5 program stars. The symbols in the figure correspond to AGB or RGB and “tip” stars as well as the observatory used for each observation. The error bars correspond to $(\sigma_{\text{FeI}}^2 + \sigma_{\text{FeII}}^2)^{1/2}$.

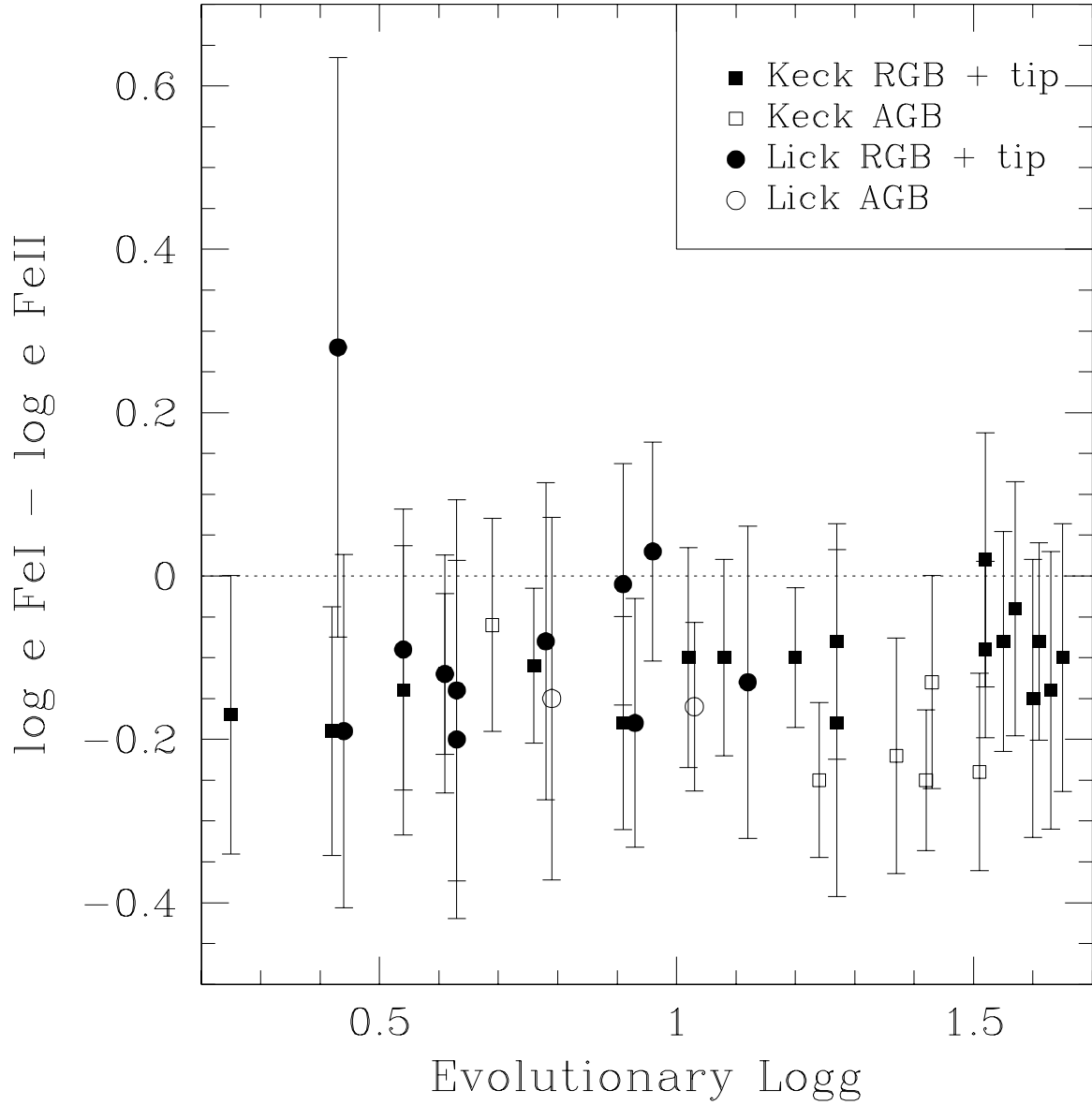


Fig. 3.— $\log \epsilon$ (Fe I) *minus* $\log \epsilon$ (Fe II) as function of $\log g$ (evolutionary). The symbols correspond to those of Figure 2.

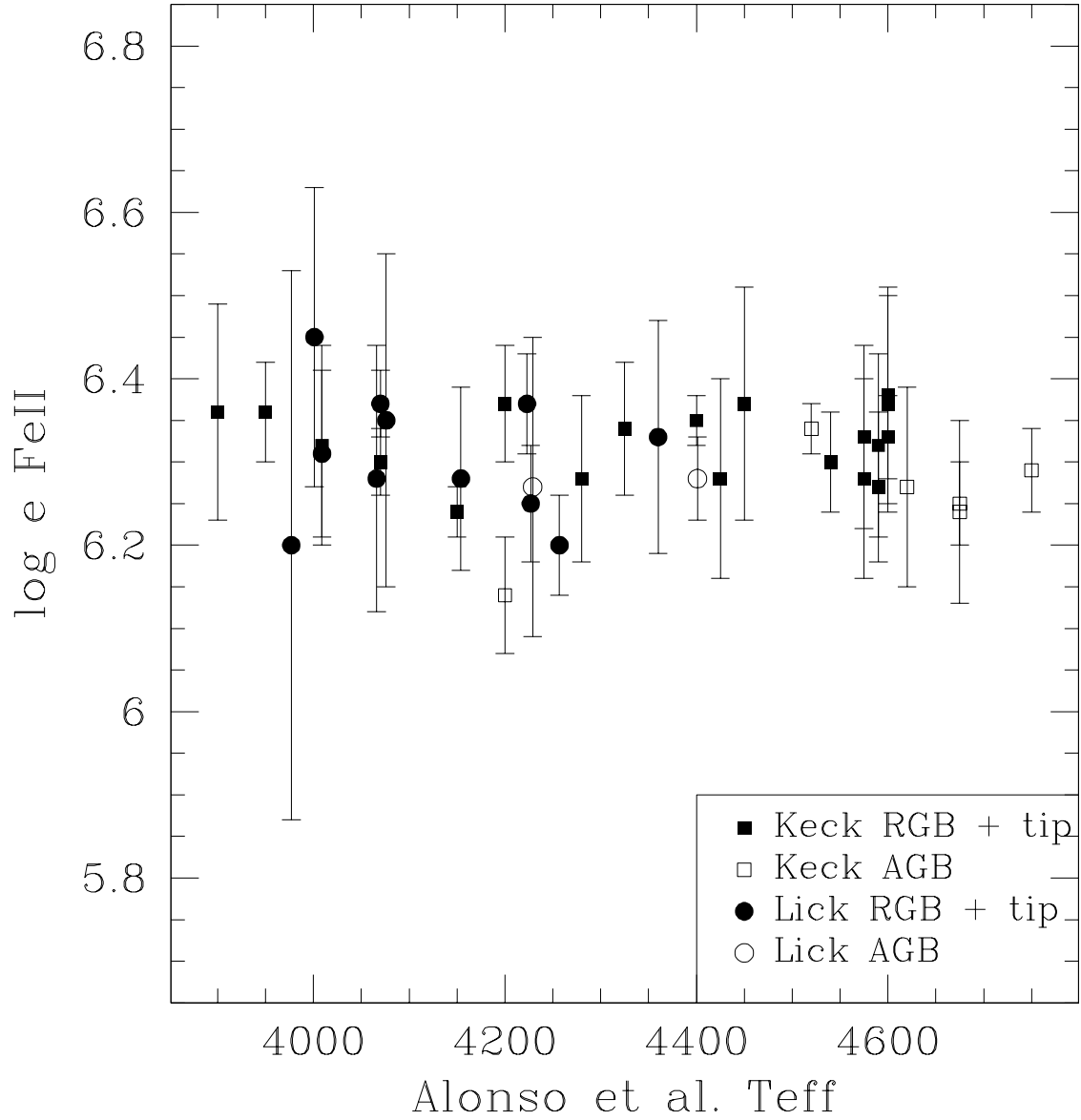


Fig. 4.— $\log \epsilon(\text{Fe II})$ as function of T_{eff} (Alonso *et al.* 1999 scale). The symbols correspond to those of Figure 2.

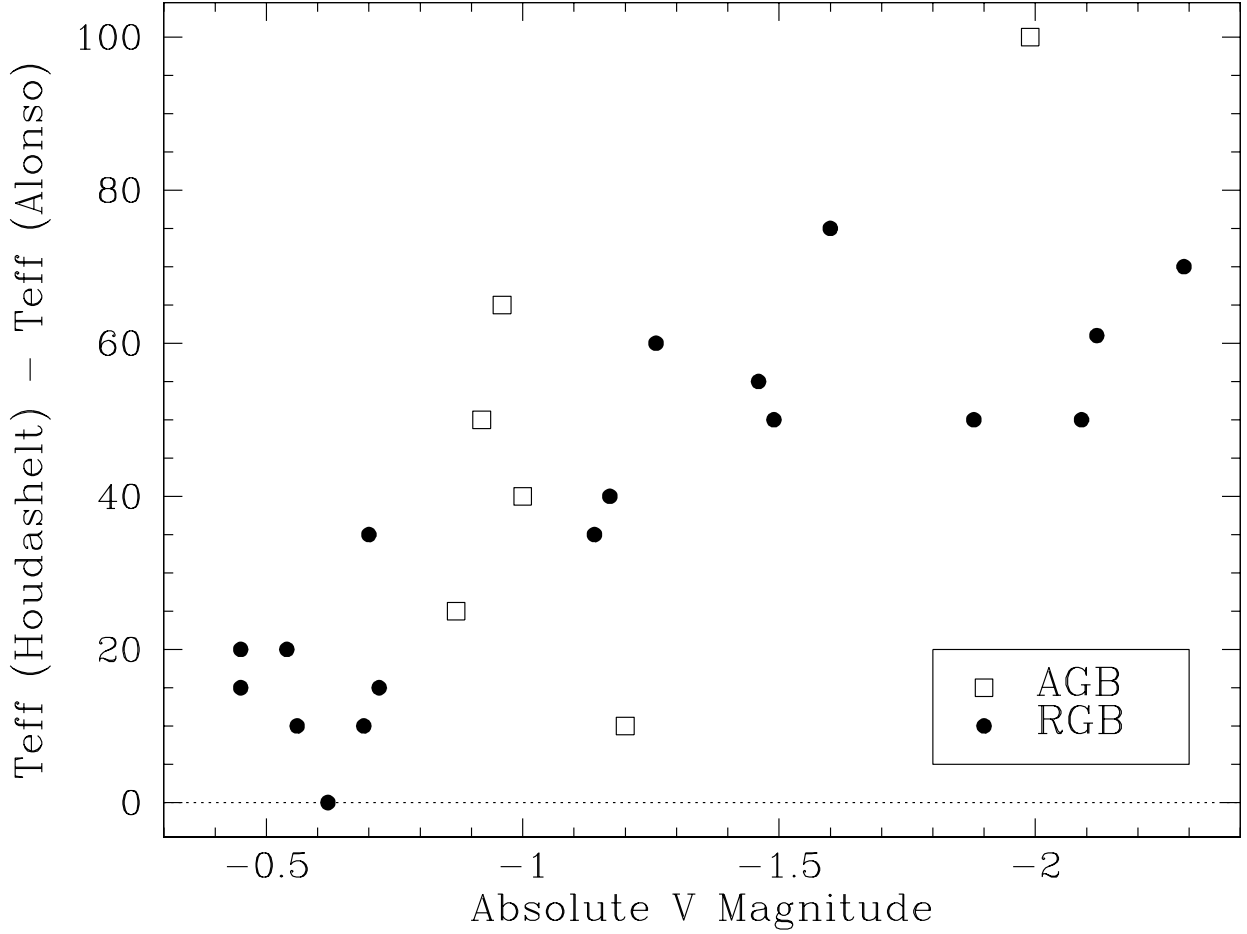


Fig. 5.— T_{eff} derived using the Houdashelt *et al.* (2000) calibration *minus* the T_{eff} derived from the Alonso *et al.* (1999) calibration as a function of the absolute V magnitude (as derived from the calibration of Alonso *et al.* 1999) for our M5 program stars observed at Keck. The symbols in the figure correspond to AGB or RGB plus “tip” stars.

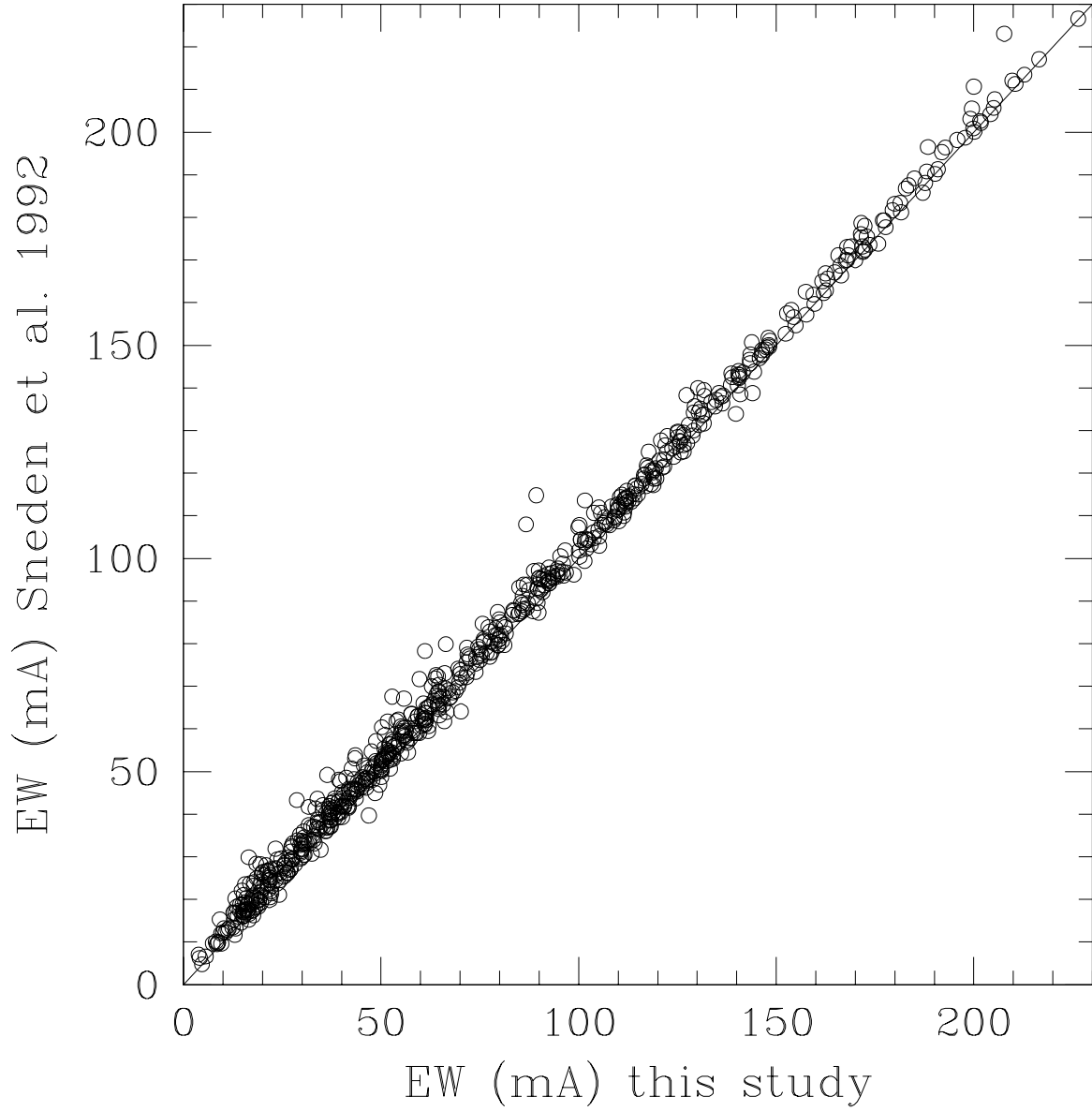


Fig. 6.— Equivalent widths for M5 giants taken from the original Lick study (Sneden *et al.* 1992) are plotted against EWs for the same lines re-measured in the Lick spectra for this study.

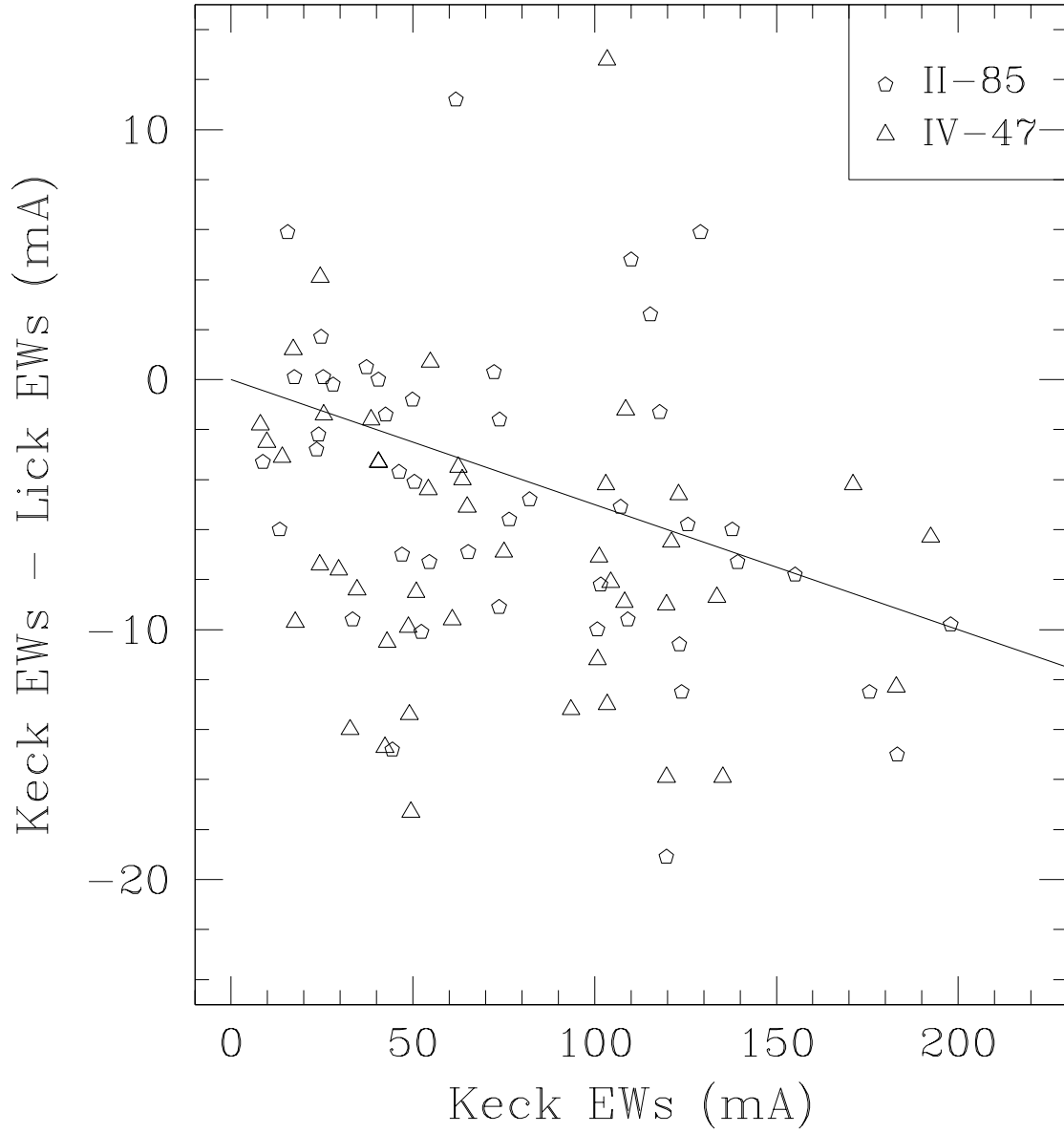


Fig. 7.— Re-measured Lick EWs for data taken prior to installation of the new Hamilton spectrograph corrector *minus* the Keck EWs as a function of Keck EWs for the two stars II-85 and IV-47. The straight line shows the 5% correction that is required to put the two data sets on to the same system.

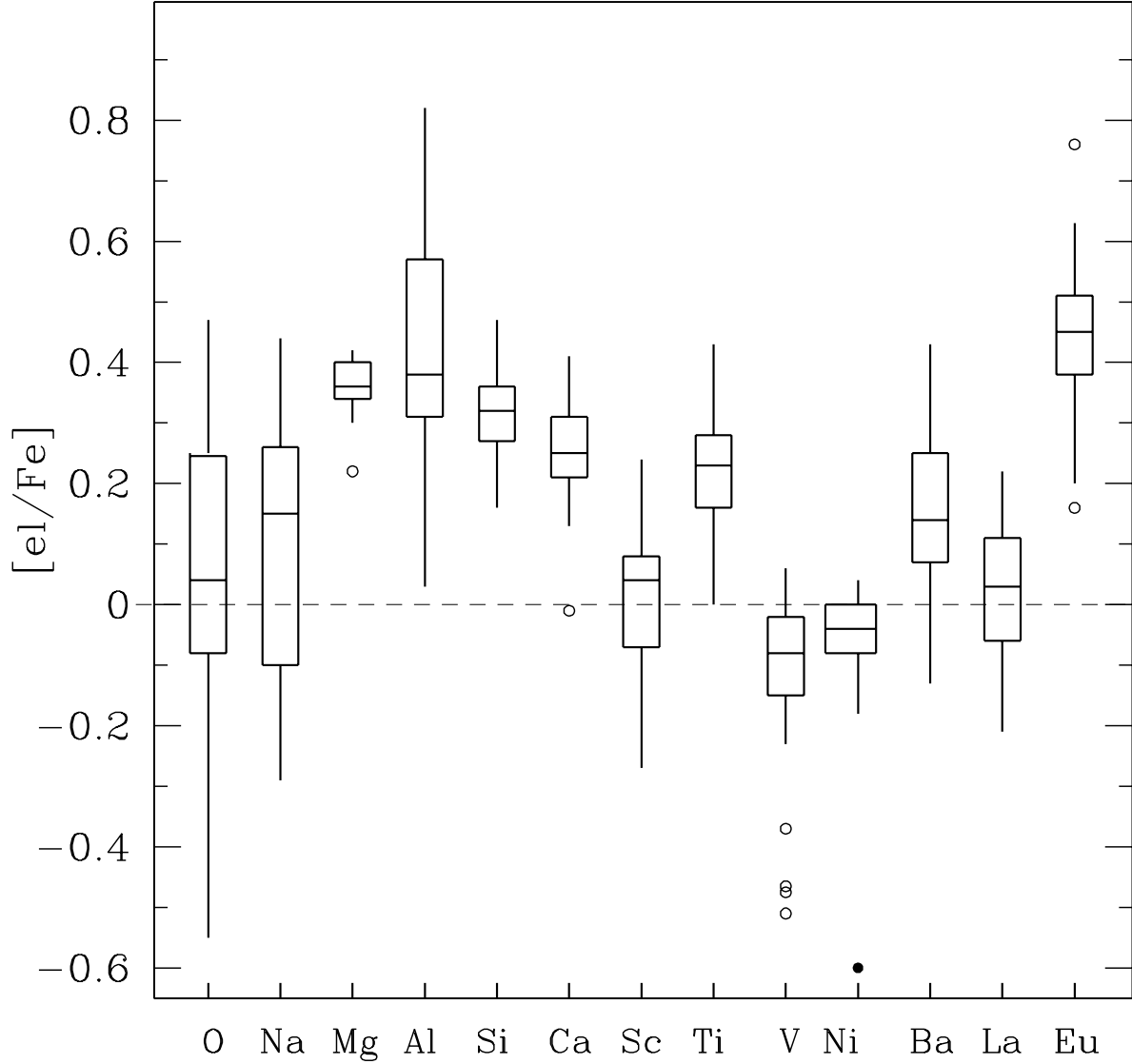


Fig. 8.— Boxplot of the M5 giant star element abundances. For all of the individual abundance boxes, the “box” contains the middle 50% of the data (ie. the interquartile range) and the horizontal line inside the box indicates the median value of a particular element. The vertical tails extending from the boxes indicate the total range of abundances determined for each element, excluding outliers. Mild outliers (those between 1.5 and 3 times the interquartile range) are denoted by open circles. Severe outliers (those greater than 3 times the interquartile range) are denoted by filled circles.

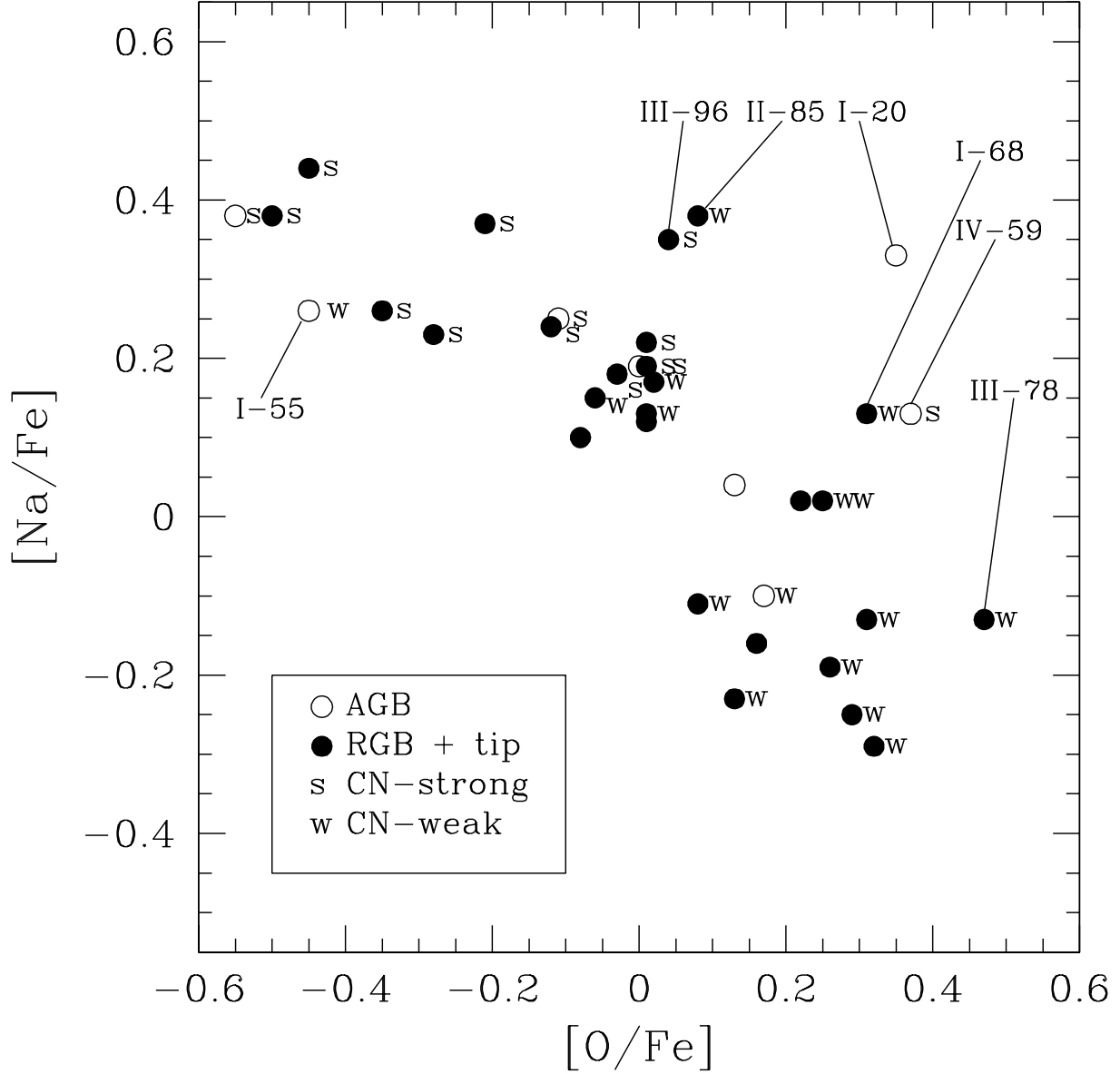


Fig. 9.— M5 sodium abundances (determined by averaging the abundances derived by syntheses of the $\lambda\lambda 5682, 5688 \text{ \AA}$ and EW abundance derived from $\lambda\lambda 6154, 6161 \text{ \AA}$ features) plotted versus oxygen abundances (determined by spectrum syntheses of the $\lambda\lambda 6300, 6364 \text{ \AA}$ features). We bin all of the stars by evolutionary state (AGB or RGB and “tip”) and 30 of the stars by CN bandstrength (CN-strong or CN-weak). Some stars stand out, are marked with individual star names and are discussed in §7.1 and 7.2.

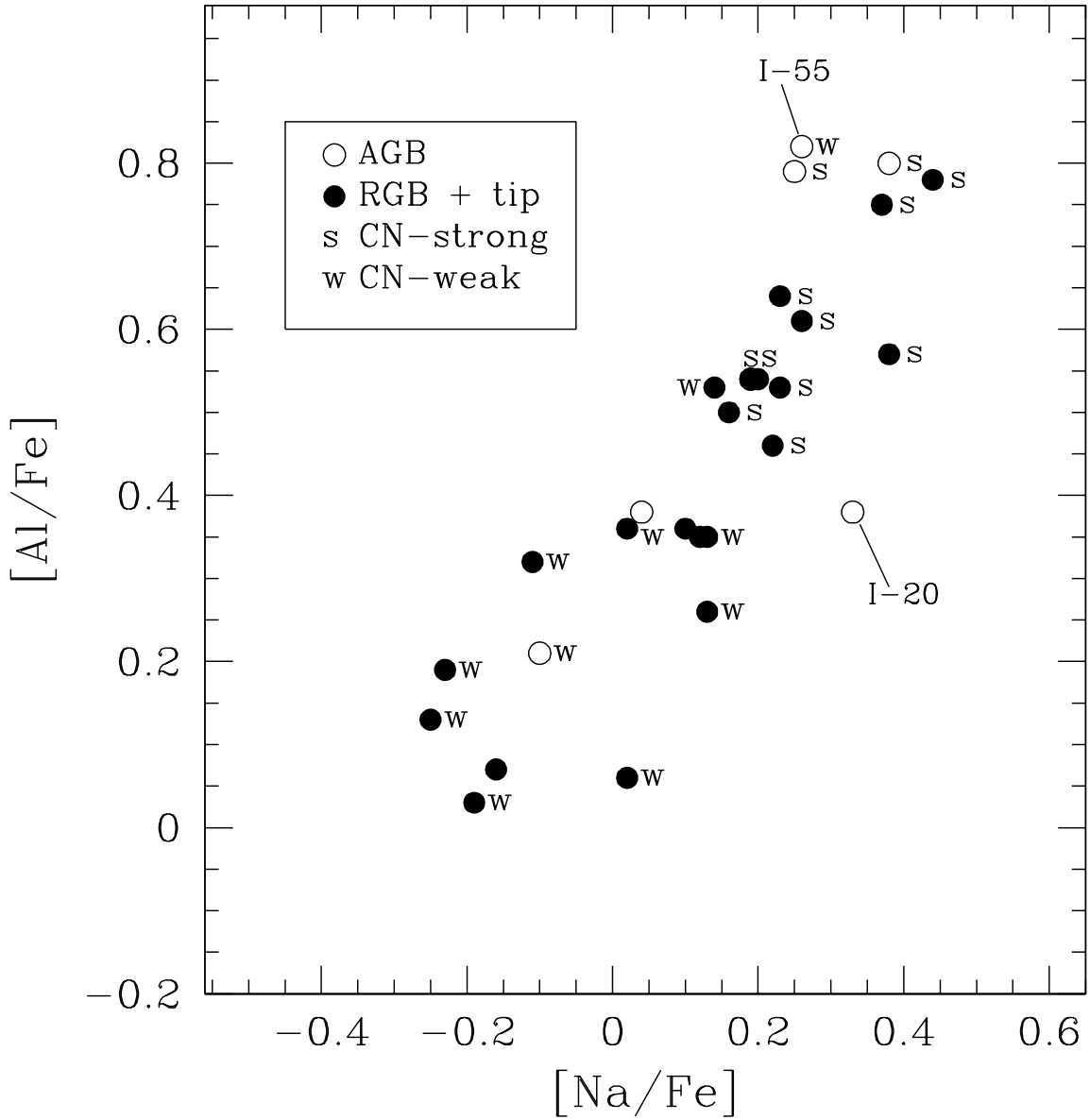


Fig. 10.— M5 aluminum abundances plotted versus sodium. Our M5 program stars show the “classic” anti-correlations and correlations seen in the brighter stars, as well as in other clusters observed by the Lick-Texas group. Stars are marked as those of Figure 9.

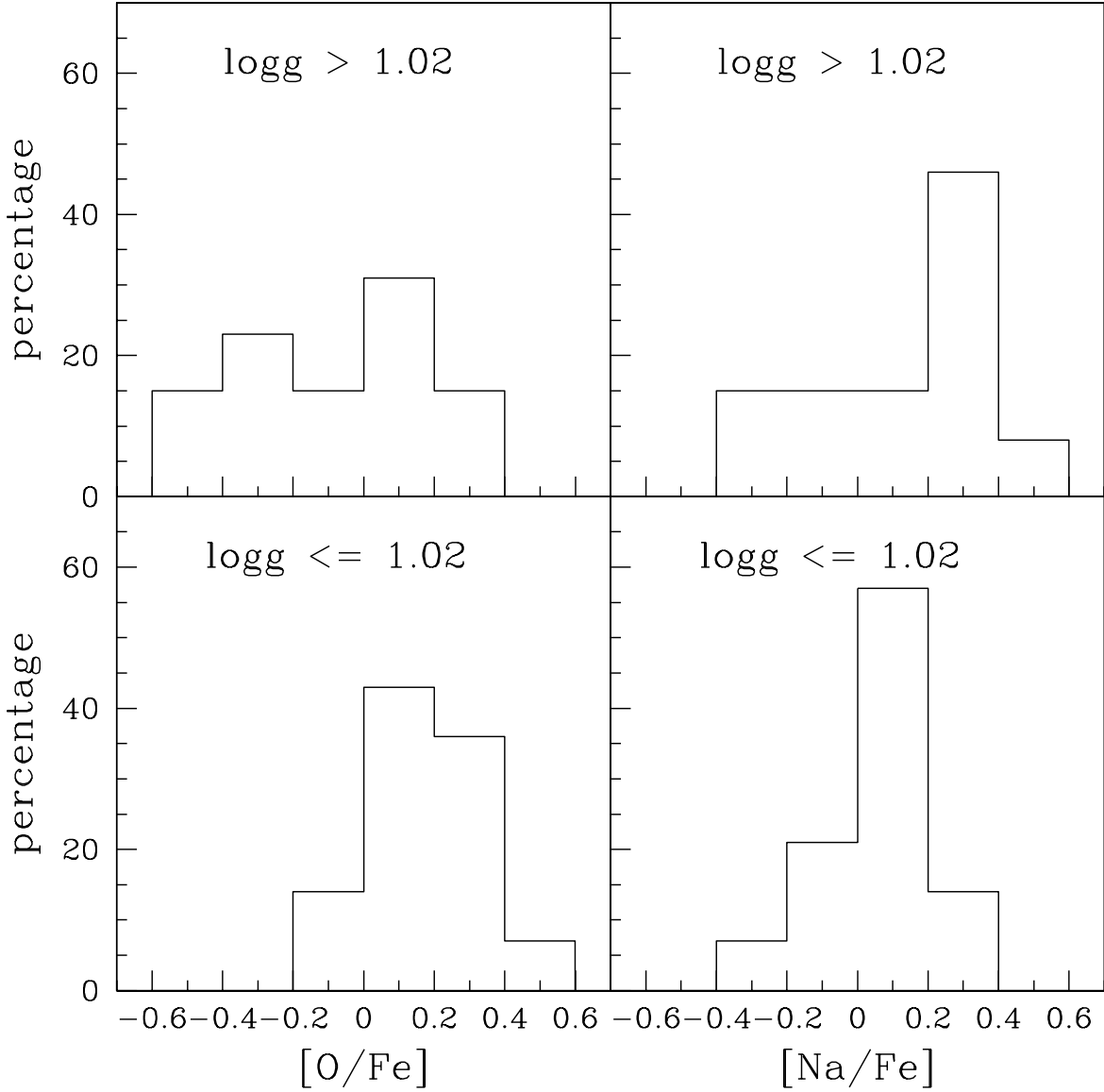


Fig. 11.— Four histograms of $[O/Fe]$ (on the left) and $[Na/Fe]$ (on the right) abundance ratio distributions for our sample of M5 RGB and “tip” stars. The top panels illustrate the percentage of the 13 stars with $\log g > 1.02$ and the bottom panels illustrate the percentage of the 14 stars with $\log g \leq 1.02$. One can easily see how the distributions in these two groups change.

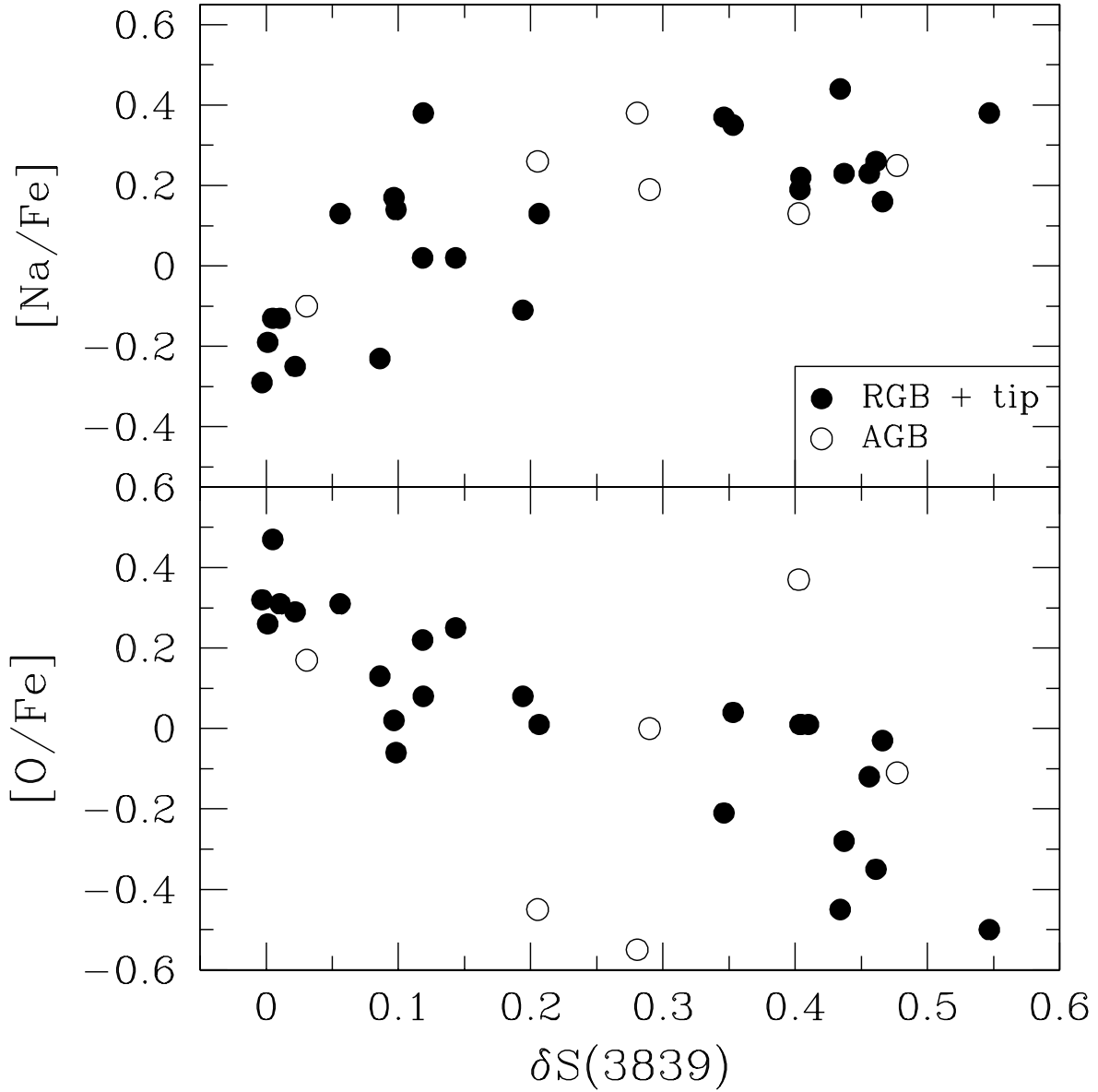


Fig. 12.— $[Na/Fe]$ and $[O/Fe]$ plotted as a function of the CN bandstrength index $\delta S(3839)$, which has been derived from the data from Smith & Norris (1983, 1993), Briley & Smith (1993) and Smith *et al.* (1997), and “detrended” for temperature effects. Stars are depicted by AGB or RGB and “tip” evolutionary state.

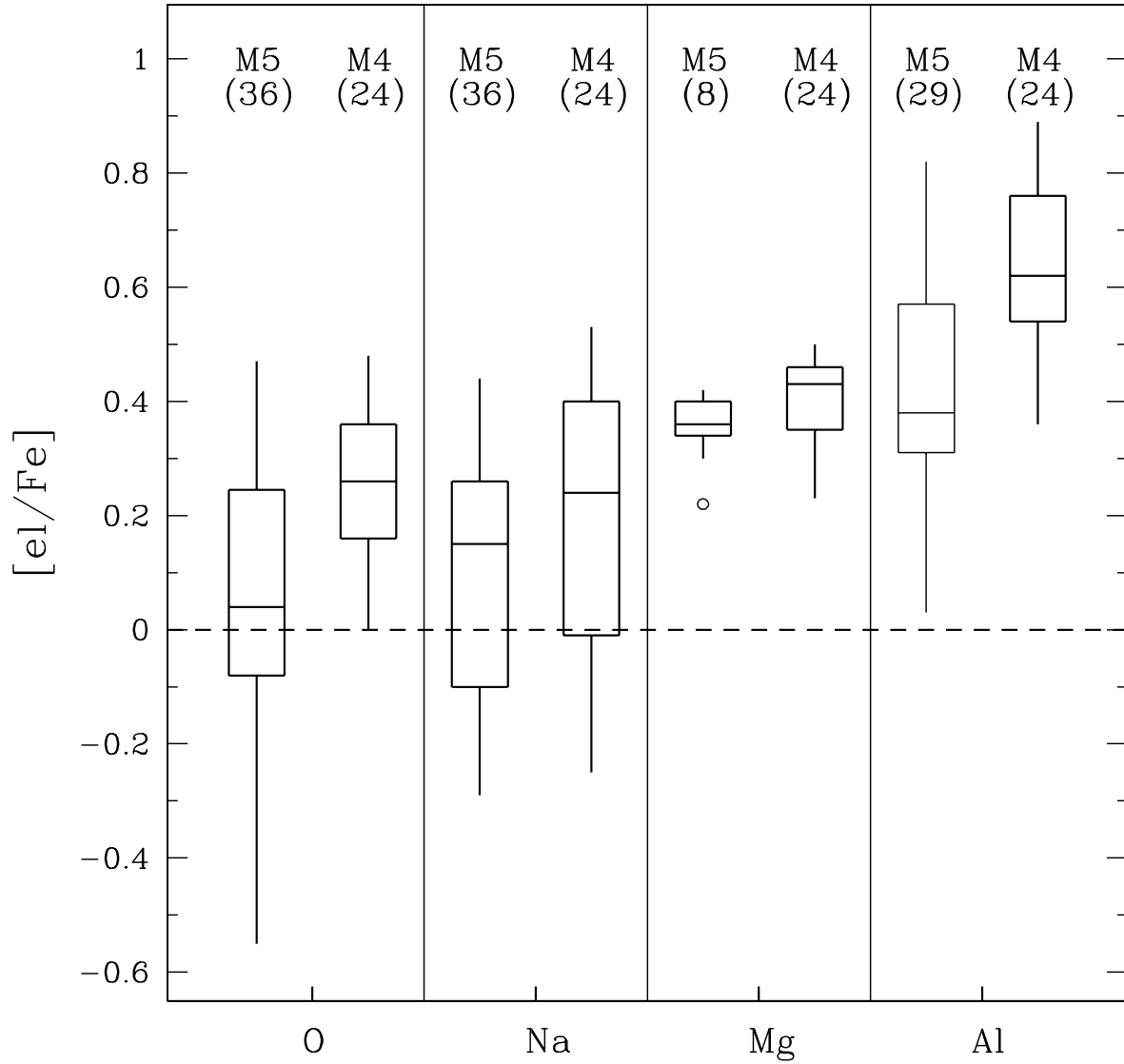


Fig. 13.— Boxplot of the M4 and M5 giant star abundances for elements which may be sensitive to proton-capture nucleosynthesis. The statistical abundance distributions represented by each box's vertical boundaries, etc., are as described in Figure 8. The number of stars included in each boxplot is noted in parentheses.

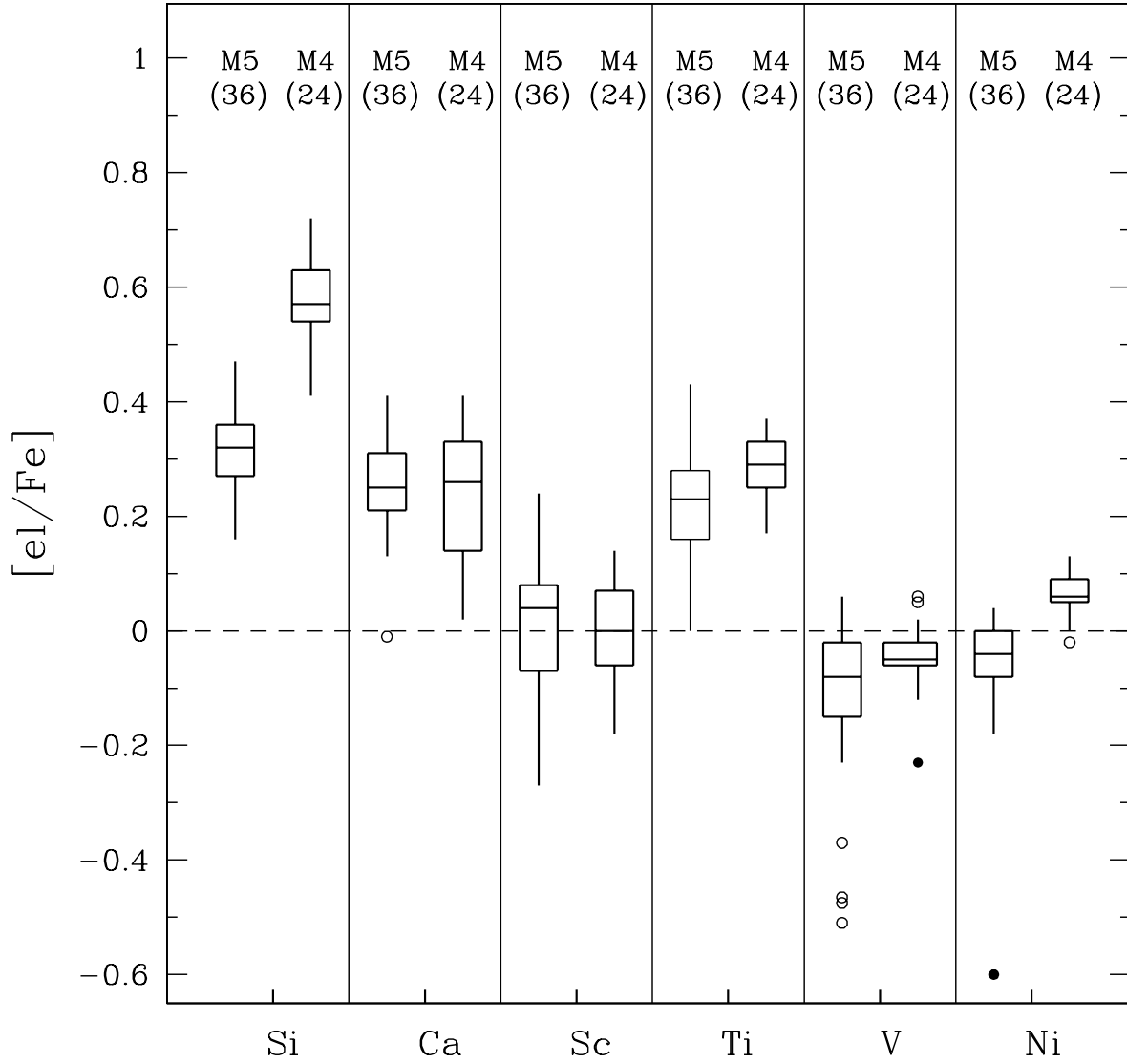


Fig. 14.— Boxplot of the M4 and M5 giant star abundances for heavier α - and Fe-peak elements. The statistical abundance distributions represented by each box's vertical boundaries, etc., are as described in Figure 8. The number of stars included in each boxplot is noted in parentheses.

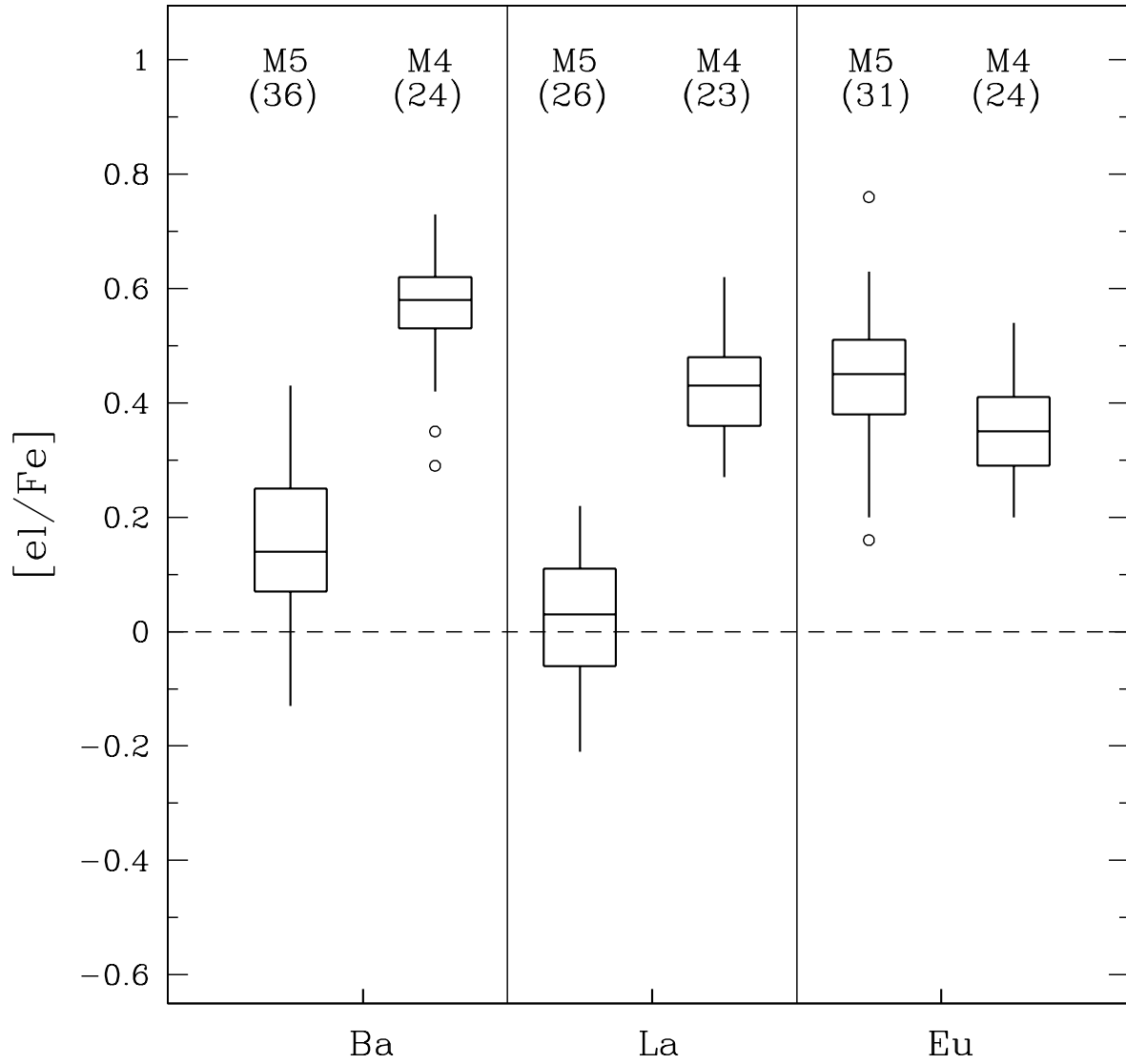


Fig. 15.— Boxplot of the M4 and M5 giant star abundances for *s*- and *r*-process elements. The statistical abundance distributions represented by each box's vertical boundaries, etc., are as described in Figure 8. The number of stars included in each boxplot is noted in parentheses.

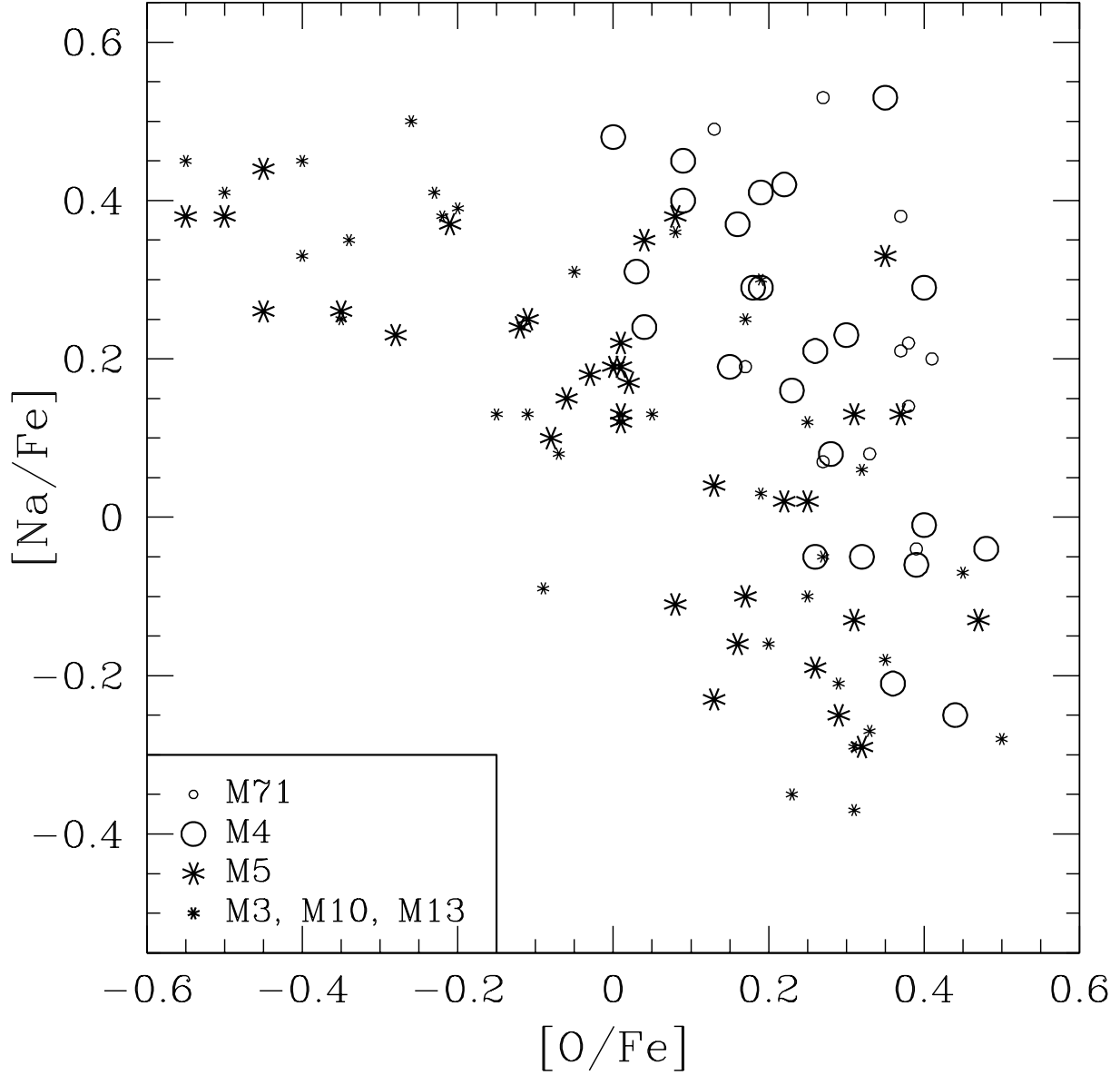


Fig. 16.— $[Na/Fe]$ versus $[O/Fe]$ for M5 and M4 and globular clusters previously studied by the Lick-Texas group that bracket M5 and M4 in metallicity. The abundance ratio anti-correlation is divided into two groups, and the symbols chosen accordingly, one for the M4-like clusters and one for the M5-like clusters.

Table 1. Photometry and Observation Log

Star	V	$B - V$	V^o	$(B - V)^o$	M_V^o	S(3839)	Instr. ¹	Date	Exp. ²	S/N ³
G2 ⁵	Keck45	1995 May 26	1500	90
IV-81	12.20	1.52	12.11	1.49	-2.29	...	Keck45	1995 05/26	1800	140
III-122	12.30	1.48	12.21	1.45	-2.19	0.309	Lick30	1990 06/03	3600	63
II-9	12.33	1.50	12.24	1.47	-2.16	...	Lick30	1990 06/04	7200	24
II-85	12.37	1.47	12.28	1.44	-2.12	0.328	Lick30	1990 06/02	4500	77
							Keck45	1998 08/15	400	62
IV-47	12.40	1.42	12.31	1.39	-2.09	0.294	Lick30	1990 05/17	5400	62
							Keck45	1998 08/16	600	65
III-3	12.44	1.41	12.35	1.38	-2.05	0.193	Lick30	1990 05/17	3600	62
I-68	12.47	1.42	12.38	1.39	-2.02	0.254	Lick30	1990 06/03	2700	67
I-20	12.50	1.31	12.41	1.28	-1.99	...	Keck45	1995 05/26	3600	65
IV-19	12.61	1.35	12.52	1.32	-1.88	0.30	Keck45	1995 05/26	1800	106
III-78	12.63	1.34	12.54	1.31	-1.86	0.186	Lick30	1990 05/17	7200	63
IV-59	12.66	1.28	12.57	1.25	-1.83	0.569	Lick30	1990 05/16	4500	60
III-36	12.81	1.29	12.72	1.26	-1.68	0.31	Lick30	1990 05/17	7200	54
III-96	12.86	1.26	12.77	1.23	-1.63	0.514	Lick30	1990 06/02	6300	68
IV-72	12.86	1.29	12.77	1.26	-1.63	0.178	Lick30	1990 06/04	7200	85
III-149	12.89	1.30	12.80	1.27	-1.60	...	Keck45	1995 05/25	1800	103
III-50	12.91	1.15	12.82	1.12	-1.58	0.61	Lick30	1990 06/04	7200	70
I-14	13.00	1.23	12.91	1.20	-1.49	0.56	Keck45	1995 05/25	1250	87
IV-34	13.03	1.21	12.94	1.18	-1.46	0.354	Keck45	1995 05/25	1800	88
I-71	13.08	1.18	12.99	1.15	-1.41	0.487	Lick30	1990 06/03	7220	54
I-58	13.23	1.15	13.14	1.12	-1.26	0.57	Keck45	1995 05/24	1800	95
III-18	13.29	1.08	13.20	1.05	-1.20	...	Keck45	1995 05/25	1800	85
II-59	13.32	1.12	13.23	1.09	-1.17	0.67	Keck45	1994 06/18	3600	25
I-61	13.35	1.14	13.26	1.11	-1.14	0.15	Keck45	1995 05/24	1800	100
IV-30	13.49	1.00	13.40	0.97	-1.00	0.38	Keck45	1995 05/25	3000	100
III-53	13.53	0.95	13.44	0.92	-0.96	0.36	Keck45	1994 06/19,20	6000	124
IV-26	13.57	0.96	13.48	0.93	-0.92	0.11	Keck45	1994 06/20	3600	100
I-55	13.62	0.93	13.53	0.90	-0.87	0.27	Keck45	1995 05/25	2500	103
II-74	13.77	1.04	13.68	1.01	-0.72	0.56	Keck45	1994 06/20	3600	92
I-2	13.79	1.05	13.70	1.02	-0.70	0.51	Keck45	1994 06/20	3600	144
I-50	13.80	1.03	13.71	1.00	-0.69	0.53	Keck45	1995 05/25	1925	111
II-50	13.87	1.03	13.78	1.00	-0.62	0.29	Keck45	1994 06/20	3600	96
IV-36	13.95	1.02	13.86	0.99	-0.54	0.56	Keck45	1994 06/19	3600	108
III-59	13.93	1.02	13.84	0.99	-0.56	0.55	Keck45	1995 05/26	1800	81
III-52	14.04	1.04	13.95	1.01	-0.45	0.10	Keck45	1994 06/18,20	5400	140
IV-4	14.04	1.01	13.95	0.98	-0.45	0.18	Keck45	1994 06/18	1800	47

²Keck45 \equiv Keck I + HIRES, $R \simeq 45,000$; Lick30 \equiv Lick 3.0m + Hamilton echelle, $R \simeq 30,000$.

³Total exposure time in seconds.

⁴S/N as measured in a line-free region near $\lambda 6300 \text{ \AA}$.

⁵See §2 for details. Only $2\mu\text{m}$ observations are available to us for this star.

Table 2. Spectroscopic and Evolutionary Model Parameters

Star	Spectroscopic ¹						Evol. ³	Evolutionary ²					
	T _{eff}	log <i>g</i>	<i>v_t</i>	log ϵ	log ϵ	[Fe/H]		T _{eff}	log <i>g</i>	<i>v_t</i>	log ϵ	log ϵ	[Fe/H]
				Fe I	Fe II	mean					Fe I	Fe II	Fe II
I-55	4700	0.85	1.80	6.04	6.05	-1.48	a	4750	1.51	1.90	6.05	6.29	-1.23
III-53	4700	1.05	1.75	6.05	6.07	-1.46	a	4675	1.42	1.75	6.00	6.25	-1.27
IV-26	4650	1.05	1.40	6.13	6.11	-1.40	a	4675	1.43	1.50	6.11	6.24	-1.28
IV-30	4625	1.00	1.75	6.07	6.09	-1.44	a	4620	1.37	1.75	6.05	6.27	-1.25
III-18	4475	0.55	1.70	6.06	6.07	-1.46	a	4520	1.24	1.80	6.09	6.34	-1.18
I-20 ⁴	4050	0.00	2.00	6.05	6.05	-1.47	a	4200	0.69	2.40	6.08	6.14	-1.38
IV-4	4625	1.55	1.20	6.27	6.28	-1.25	r	4600	1.65	1.10	6.28	6.38	-1.14
IV-36	4575	1.50	1.35	6.22	6.20	-1.30	r	4600	1.61	1.35	6.25	6.33	-1.19
III-59	4575	1.20	1.35	6.21	6.21	-1.31	r	4600	1.60	1.40	6.22	6.37	-1.15
I-50	4525	1.15	1.40	6.18	6.16	-1.35	r	4590	1.55	1.60	6.19	6.27	-1.25
II-50	4525	1.15	1.35	6.24	6.24	-1.28	r	4590	1.57	1.45	6.28	6.32	-1.20
III-52	4625	1.50	1.45	6.19	6.17	-1.34	r	4575	1.63	1.40	6.14	6.28	-1.24
II-74	4525	1.30	1.30	6.27	6.25	-1.25	r	4575	1.52	1.25	6.35	6.33	-1.19
I-2	4500	1.10	1.45	6.17	6.14	-1.36	r	4540	1.52	1.50	6.21	6.30	-1.22
II-59	4463	1.15	1.65	6.29	6.25	-1.25	r	4450	1.27	1.30	6.19	6.37	-1.15
I-61	4400	1.00	1.50	6.22	6.21	-1.30	r	4425	1.27	1.70	6.20	6.28	-1.24
I-58	4350	0.80	1.50	6.21	6.22	-1.31	r	4400	1.20	1.60	6.25	6.35	-1.17
IV-34	4275	0.65	1.55	6.20	6.20	-1.32	r	4325	1.08	1.65	6.24	6.34	-1.18
I-14	4250	0.75	1.60	6.19	6.20	-1.33	r	4280	1.02	1.75	6.18	6.28	-1.24
III-149	4225	0.60	1.70	6.20	6.18	-1.33	t	4200	0.91	1.75	6.19	6.37	-1.15
IV-19	4125	0.50	1.70	6.11	6.15	-1.39	t	4150	0.76	1.75	6.13	6.24	-1.28
IV-47	4110	0.50	1.85	6.21	6.17	-1.33	t	4070	0.61	1.90	6.18	6.30	-1.22
II-85	4050	0.45	1.85	6.18	6.20	-1.33	t	4009	0.54	1.85	6.18	6.32	-1.20
IV-81	3945	0.00	1.90	6.11	6.14	-1.39	t	3950	0.42	1.90	6.17	6.36	-1.16
G2 ⁵	3900	-0.10	1.75	6.16	6.18	-1.35	t	3900	0.25	1.80	6.19	6.36	-1.16

¹Spectroscopic parameters: T_{eff} from excitation and log *g* from ionization equilibria, *v_t* from trends in EW

²Evolutionary parameters: T_{eff} from Alonso et al. (1999), log *g* from cluster photometry, *v_t* from trends in EW

³Estimated evolutionary state: a ≡ AGB, r ≡ RGB, t ≡ RGB tip

⁴The coolest AGB star

⁵No photometry available; see text

Table 3. Abundance Dependencies on Model Atmosphere Parameters

Abundance	ΔT_{eff} $\pm 50 \text{ K}$	$\Delta \log g$ ± 0.20	Δv_t ± 0.20	$\Delta [\text{M}/\text{H}]$ ± 0.20	$\Delta \text{m-M}$ ± 0.50	$\Delta \mathcal{M}$ ± 0.10
[Fe I/H]	± 0.04	± 0.02	∓ 0.09	± 0.02	∓ 0.02	± 0.01
[Fe II/H]	∓ 0.06	± 0.11	∓ 0.04	± 0.08	∓ 0.11	± 0.03
[O I/Fe II]	± 0.05	∓ 0.03	± 0.03	∓ 0.04	± 0.03	∓ 0.01
[Na I/Fe I]	± 0.01	∓ 0.04	± 0.05	± 0.01	± 0.04	∓ 0.02
[Mg I/Fe I]	± 0.00	∓ 0.06	± 0.01	∓ 0.01	± 0.06	∓ 0.02
[Al I/Fe I]	± 0.00	∓ 0.03	± 0.08	± 0.01	± 0.03	∓ 0.01
[Si I/Fe I]	∓ 0.06	± 0.02	± 0.08	∓ 0.02	∓ 0.02	± 0.01
[Ca I/Fe I]	± 0.02	∓ 0.03	± 0.01	± 0.03	± 0.03	∓ 0.01
[Sc II/Fe II]	± 0.05	∓ 0.03	∓ 0.04	∓ 0.07	± 0.03	∓ 0.01
[Ti I/Fe I]	± 0.06	∓ 0.03	± 0.03	± 0.03	± 0.03	∓ 0.01
[Ti II/Fe II]	± 0.04	∓ 0.02	± 0.01	∓ 0.07	± 0.02	∓ 0.01
[V I/Fe I]	± 0.06	∓ 0.03	± 0.06	± 0.04	± 0.03	∓ 0.01
[Mn I/Fe I]	± 0.03	∓ 0.03	∓ 0.02	± 0.02	± 0.03	∓ 0.01
[Ni I/Fe I]	∓ 0.02	± 0.01	± 0.03	∓ 0.02	∓ 0.01	± 0.01
[Ba II/Fe II]	± 0.07	∓ 0.04	∓ 0.14	∓ 0.10	± 0.04	∓ 0.01
[La II/Fe II]	± 0.07	∓ 0.11	± 0.03	∓ 0.07	± 0.11	∓ 0.01
[Eu II/Fe II]	± 0.05	∓ 0.02	± 0.01	∓ 0.08	± 0.04	∓ 0.01

¹Baseline model: $T_{\text{eff}} = 4325 \text{ K}$, $\log g = 1.08$, $v_t = 1.65$, $[\text{M}/\text{H}] = -1.00$

Table 4. A Comparison of Atmospheric Parameters: Alonso et al. vs. Houdashelt et al.

Star	M_V^c	Evol. ^a	T_{eff} HBS ^b	T_{eff} AAM	$\log g$ HBS	$\log g$ AAM	$\delta[\text{Fe}/\text{H}]^c$ HBS	$\delta[\text{Fe}/\text{H}]$ AAM	$[\text{Fe II}/\text{H}]$ HBS	$[\text{Fe II}/\text{H}]$ AAM
II4	-1.47	r	4330	4280	1.09	1.02	+0.04	+0.10	-1.27	-1.18
I50	-0.69	r	4600	4590	1.65	1.55	+0.08	+0.08	-1.25	-1.25
IV36	-0.56	r	4620	4600	1.66	1.61	+0.07	+0.07	-1.19	-1.19
II85	-2.12	t	4070	4009	0.64	0.54	+0.01	+0.14	-1.24	-1.20
IV47	-2.09	t	4120	4070	0.69	0.61	+0.12	+0.12	-1.25	-1.22
IV19	-1.88	t	4200	4150	0.84	0.76	+0.07	+0.11	-1.32	-1.28
IV30	-1.00	a	4660	4620	1.44	1.37	+0.08	+0.22	-1.26	-1.25
III53	-0.96	a	4740	4675	1.50	1.42	+0.17	+0.25	-1.29	-1.27
I55	-0.87	a	4775	4750	1.56	1.51	+0.22	+0.24	-1.23	-1.23

Mean Iron Abundance Differences by Evolutionary State

$\langle \rangle$	r	+0.06	+0.12	-1.24	-1.23
σ	r	0.02	0.02	0.04	0.04
$\langle \rangle$	t	+0.07	+0.12	-1.27	-1.23
σ	t	0.06	0.02	0.04	0.04
$\langle \rangle$	a	+0.16	+0.12	-1.26	-1.23
σ	a	0.07	0.02	0.03	0.04

^aEstimated evolutionary state: a \equiv AGB, r \equiv RGB, t \equiv RGB tip, all \equiv all stars.

^bHBS \equiv Houdashelt *et al.* (2000), and AAM \equiv Alonso *et al.* (1999).

^cThis is the difference in the sense $\log \epsilon(\text{Fe II})$ minus $\log \epsilon(\text{Fe I})$.

Table 5. Metallicities and Abundance Ratios for Stars Observed at Keck

Star	Evol. ¹	Fe ² II ³	Fe I	O II	Na I	Mg I	Al I	Si I	Ca I	Sc II	Ti I	V I	Mn I	Ni I	Ba II	La II	Eu II	Ba/Eu II
I-55	a	-1.23	-1.47	-0.45	+0.26	...	+0.82	+0.35	+0.24	+0.01	+0.18	-0.36	-0.44	0.00	+0.24	-0.03	+0.26	-0.02
III-53	a	-1.27	-1.52	-0.55	+0.38	...	+0.80	+0.44	+0.23	-0.04	+0.11	-0.46	-0.36	-0.05	+0.37	-0.07	+0.41	-0.04
IV-26	a	-1.28	-1.41	+0.17	-0.10	...	+0.21	+0.31	+0.33	-0.01	+0.12	-0.09 ⁵	-0.31	-0.06	+0.32	-0.05	+0.49	-0.17
IV-30	a	-1.25	-1.47	0.00	+0.19	...	+0.54	+0.36	+0.25	+0.04	+0.18	-0.17	-0.34	0.00	+0.25	-0.08	+0.33	-0.08
III-18	a	-1.18	-1.43	+0.13	+0.04	...	+0.38	+0.32	+0.23	-0.03	+0.14	-0.05	-0.30	0.00	+0.16	-0.21	+0.27	-0.11
L-20	a	-1.38	-1.44	+0.35	+0.33	...	+0.38	+0.47	+0.19	+0.04	+0.30	+0.03	-0.29	-0.01	+0.21	0.00	+0.49	-0.28
IV-4 ⁴	r	-1.14	-1.24	+0.13	-0.23	...	+0.19	+0.20	+0.35	+0.11	+0.12	-0.22	-0.36	+0.02	+0.43	+0.22	+0.20	+0.23
IV-36	r	-1.19	-1.27	-0.03	+0.18	...	+0.50	+0.26	+0.31	+0.14	+0.21	0.00	-0.25	-0.06	+0.28	-0.03	+0.51	-0.23
III-59	r	-1.15	-1.30	-0.12	+0.24	...	+0.64	+0.32	+0.34	-0.11	+0.28	-0.10	-0.18	-0.04	+0.14	+0.12	+0.45	-0.31
I-50	r	-1.25	-1.33	-0.45	+0.44	...	+0.78	+0.26	+0.32	+0.08	+0.24	0.00	-0.20	-0.01	+0.12	+0.15	+0.54	-0.42
II-50	r	-1.20	-1.24	+0.08	-0.11	...	+0.32	+0.24	+0.26	+0.04	+0.21	-0.11	-0.21	-0.12	+0.23	+0.19	+0.49	-0.26
III-52	r	-1.24	-1.38	+0.26	-0.19	...	+0.03	+0.34	+0.35	+0.05	+0.20	-0.03	-0.22	0.00	+0.21	+0.03	+0.52	-0.31
II-74	r	-1.19	-1.17	-0.35	+0.26	...	+0.61	+0.26	+0.28	+0.24	+0.13	-0.12	-0.15	-0.08	+0.37	+0.11	+0.53	-0.16
I-2	r	-1.22	-1.31	+0.01	+0.22	...	+0.46	+0.34	+0.33	+0.11	+0.26	-0.11	-0.28	-0.06	+0.16	+0.08	+0.49	-0.33
II-59 ⁴	r	-1.15	-1.33	-0.50	+0.38	...	+0.57	+0.37	+0.41	+0.05	+0.04	-0.47	-0.36	-0.10	+0.03	-0.15	+0.16	-0.13
I-61	r	-1.24	-1.32	+0.29	-0.25	...	+0.13	+0.31	+0.30	+0.06	+0.24	+0.03	-0.22	-0.06	+0.14	+0.20	+0.59	-0.45
I-58	r	-1.17	-1.27	-0.28	+0.23	...	+0.53	+0.30	+0.32	+0.09	+0.23	-0.01	-0.20	-0.03	+0.16	+0.06	+0.41	-0.25
IV-34	r	-1.18	-1.28	+0.01	+0.13	...	+0.35	+0.28	+0.27	+0.05	+0.28	-0.02	-0.24	-0.03	+0.17	-0.12	+0.45	-0.28
I-14	r	-1.24	-1.34	+0.01	+0.19	...	+0.54	+0.36	+0.25	+0.12	+0.21	-0.03	-0.23	-0.04	+0.05	+0.15	+0.46	-0.41
III-149	t	-1.15	-1.33	+0.16	-0.16	...	+0.07	+0.33	+0.25	-0.03	+0.16	-0.07	-0.24	-0.05	+0.09	-0.07	+0.45	-0.36
IV-19	t	-1.28	-1.39	+0.22	+0.02	...	+0.36	+0.37	+0.30	+0.05	+0.31	+0.03	-0.20	+0.02	+0.12	+0.09	+0.52	-0.40
IV-47	t	-1.22	-1.34	+0.02	+0.17	+0.36	...	+0.27	+0.21	-0.01	+0.23	+0.02	...	-0.05	+0.07	+0.03	+0.37	-0.30
II-85	t	-1.20	-1.34	+0.08	+0.38	+0.42	...	+0.38	+0.25	-0.07	+0.18	-0.02	...	-0.02	0.00	-0.01	+0.36	-0.36
IV-81	t	-1.16	-1.35	-0.08	+0.10	...	+0.36	+0.37	+0.23	0.00	+0.29	+0.01	-0.15	-0.03	+0.07	+0.03	+0.39	-0.32
G2	t	-1.16	-1.33	+0.01	+0.12	...	+0.35	+0.30	+0.23	-0.07	+0.41	-0.08	-0.04	-0.01	+0.07	-0.06	+0.38	-0.31
Mean Abundances by Evolutionary State																		
<>	a	-1.27	-1.46	-0.06	+0.18	...	+0.52	+0.38	+0.24	0.00	+0.17	-0.18	-0.34	-0.02	+0.26	-0.07	+0.38	-0.12
σ	a	0.07	0.04	0.36	0.18	...	0.25	0.07	0.05	0.03	0.07	0.19	0.06	0.03	0.08	0.07	0.10	0.10
<>	r	-1.20	-1.29	-0.07	+0.11	...	+0.43	+0.30	+0.31	0.08	+0.20	-0.09	-0.24	-0.05	+0.19	+0.08	+0.45	-0.25
σ	r	0.04	0.05	0.25	0.23	...	0.22	0.05	0.04	0.08	0.07	0.13	0.06	0.04	0.11	0.12	0.13	0.17
<>	r+t	-1.20	-1.31	-0.03	+0.11	+0.39	+0.40	+0.31	+0.29	0.05	+0.22	-0.07	-0.22	-0.04	+0.15	+0.05	+0.44	-0.28
σ	r+t	0.05	0.05	0.23	0.21	0.04	0.21	0.05	0.05	0.08	0.08	0.12	0.07	0.04	0.11	0.11	0.11	0.15
<>	all	-1.21	-1.34	-0.04	+0.12	+0.39	+0.43	+0.32	+0.28	+0.04	+0.21	-0.10	-0.25	-0.03	+0.18	+0.02	+0.42	-0.24
σ	all	0.06	0.08	0.26	0.20	0.04	0.22	0.06	0.05	0.08	0.08	0.14	0.09	0.04	0.11	0.11	0.11	0.15

¹Estimated evolutionary state: a \equiv AGB, r \equiv RGB, t \equiv RGB tip, all \equiv all stars.

²Column headings labeled "Fe" stand for [Fe/H] values; headings labeled with other element symbols "X" stand for [X/Fe] values; and the heading labeled "Ba/Eu" stands for [Ba/Eu].

³"II" means [Fe/H] derived from Fe II lines or [e]/[Fe] ratios referred to the Fe II metallicity values; "I" means these same quantities but employing the Fe I lines.

⁴Abundances for II-59 and IV-4 have low weight; their spectra have S/N < 50.

⁵Hyperfine structure calculations were not possible for V I in this star; the abundance given here is that from EW single-line calculations, reduced by 0.06 dex (the mean reduction from hyperfine structure syntheses for other AGB stars).

Table 6. Re-analyzed Metallicities and Abundance Ratios for Stars Observed at Lick

Star	Evol. ¹	[Fe/H] II ²	[Fe/H] I	[O/Fe] II	[Na/Fe] I	[Si/Fe] I	[Ca/Fe] I	[Sc/Fe] II	[Ti/Fe] I	[V/Fe] I	[Ni/Fe] I	[Ba/Fe] II	T _{eff}	log <i>g</i>	<i>v_t</i>
III-50	a	-1.24	-1.40	-0.11	+0.25	+0.38	+0.21	-0.21	+0.08	-0.14	-0.04	+0.32	4401	1.03	1.85
IV-59	a	-1.25	-1.40	+0.37	+0.13	+0.23	+0.21	-0.19	+0.02	-0.21	-0.14	+0.10	4229	0.79	2.10
I-71	t	-1.19	-1.32	-0.21	+0.37	+0.38	+0.24	-0.17	+0.25	-0.05	-0.09	+0.08	4360	1.12	1.65
III-96	t	-1.32	-1.29	+0.04	+0.35	+0.27	+0.26	+0.10	+0.24	-0.16	-0.16	+0.33	4257	0.96	1.55
IV-72 ³	t	-1.15	-1.33	+0.31	-0.13	+0.36	+0.14	-0.27	+0.27	-0.12	-0.11	+0.10	4223	0.93	1.60
III-36	t	-1.27	-1.28	+0.25	+0.02	+0.22	+0.19	+0.06	+0.21	-0.12	-0.14	+0.30	4227	0.91	1.65
III-78	t	-1.24	-1.32	+0.47	-0.13	+0.35	+0.19	+0.14	+0.32	-0.03	+0.04	+0.04	4154	0.78	1.95
III-3	t	-1.17	-1.31	+0.32	-0.29	+0.22	+0.21	-0.21	+0.30	-0.05	+0.02	-0.01	4076	0.63	1.95
I-68	t	-1.24	-1.44	+0.31	+0.13	+0.27	+0.18	-0.19	+0.43	+0.07	+0.03	-0.11	4066	0.63	2.20
III-122	t	-1.07	-1.26	-0.06	+0.15	+0.16	+0.13	-0.15	+0.26	-0.15	-0.18	-0.03	4001	0.44	2.00
II-9 ⁴	t	-1.32	-1.04	+0.21	-0.16	+0.30	-0.01	-0.06	0.00	-0.50	-0.60	-0.13	3977	0.43	1.25
II-85	t	-1.21	-1.30	+0.23	+0.26	+0.33	+0.14	-0.22	+0.23	-0.12	-0.07	-0.07	4009	0.54	1.80
IV-47	t	-1.15	-1.27	+0.14	+0.07	+0.19	+0.16	-0.14	+0.19	-0.12	-0.11	+0.06	4070	0.61	1.70
Mean Abundances by Evolutionary State															
<>	a	-1.25	-1.40	+0.13	+0.19	+0.31	+0.21	-0.20	+0.05	-0.18	-0.09	+0.21			
σ	a	0.01	0.00	0.34	0.08	0.11	0.00	0.01	0.04	0.05	0.07	0.16			
<>	all	-1.21	-1.33	+0.17	+0.10	+0.28	+0.19	-0.12	+0.23	-0.10	-0.08	+0.09			
σ	all	0.07	0.06	0.20	0.20	0.08	0.04	0.14	0.11	0.07	0.08	0.15			

¹Estimated evolutionary state: a \equiv AGB, t \equiv RGB and tip, all \equiv all stars.

²“II” means [Fe/H] derived from Fe II lines or [e]/[Fe] ratios referred to the Fe II metallicity values; “I” means these same quantities but employing the Fe I lines.

³Na abundances for star IV-72 are derived only from syntheses of the $\lambda\lambda 5622, 5688$ Å lines.

⁴The spectrum of II-9 has low S/N and so its abundances are excluded for the calculations of the mean abundances.

Table 7. Re-analyzed Data of Shetrone (1996)

Star	[Mg/Fe]	[Al/Fe]	[Eu/Fe]
III-50	0.34	0.79	0.45
I-71	0.40	0.75	0.48
III-3	0.36	0.06	0.47
I-68	0.30	0.26	0.63
III-122	0.22	0.53	0.35

Mean Values, Shetrone EWs			
$\langle \rangle$	0.32	0.48	0.48
\pm	0.03	0.14	0.04
σ	0.07	0.31	0.10
No.	5	5	5

Mean Values, this paper's EWs			
$\langle \rangle$	0.39	0.43	0.42
\pm	0.03	0.05	0.02
σ	0.04	0.22	0.11
No.	2	23	25

Table 8. Mean Abundances for the Entire M5 Sample

Star	Evol. ¹	Fe II ²	Fe I	O II	Na I	Mg I	Al I	Si I	Ca I	Sc II	Ti I	V I	Mn I	Ni I	Ba II	La II	Eu II	Ba/Eu II
$\langle \rangle$	a	-1.26	-1.44	-0.01	+0.19	+0.34	+0.56	+0.36	+0.24	-0.05	+0.14	-0.19	-0.34	-0.04	+0.25	-0.07	+0.39	-0.12
\pm	a	0.02	0.01	0.12	0.06	...	0.09	0.03	0.01	0.03	0.03	0.06	0.02	0.02	0.03	0.03	0.04	0.04
σ	a	0.06	0.04	0.34	0.16	...	0.25	0.08	0.04	0.10	0.08	0.16	0.06	0.05	0.09	0.07	0.10	0.10
$\langle \rangle$	r	-1.20	-1.29	-0.07	+0.11	...	+0.43	+0.30	+0.31	+0.08	+0.20	-0.10	-0.24	-0.05	+0.19	+0.08	+0.45	-0.25
\pm	r	0.01	0.02	0.07	0.06	...	0.06	0.01	0.01	0.02	0.02	0.04	0.02	0.01	0.03	0.03	0.04	0.05
σ	r	0.04	0.05	0.25	0.23	...	0.22	0.05	0.04	0.08	0.07	0.13	0.06	0.04	0.11	0.12	0.13	0.17
$\langle \rangle$	r+t	-1.20	-1.31	+0.03	+0.09	+0.34	+0.40	+0.30	+0.26	+0.01	+0.24	-0.08	-0.22	-0.05	+0.13	+0.05	+0.44	-0.32
\pm	r+t	0.01	0.01	0.05	0.04	0.03	0.05	0.01	0.02	0.02	0.02	0.02	0.02	0.01	0.03	0.02	0.03	0.04
σ	r+t	0.05	0.05	0.24	0.21	0.07	0.22	0.06	0.07	0.12	0.08	0.10	0.07	0.06	0.13	0.11	0.11	0.17
$\langle \rangle$	all	-1.21	-1.34	+0.02	+0.11	+0.34	+0.44	+0.31	+0.26	-0.01	+0.22	-0.10	-0.25	-0.05	+0.16	+0.02	+0.43	-0.27
\pm	all	0.01	0.01	0.04	0.03	0.03	0.05	0.01	0.01	0.02	0.02	0.02	0.02	0.01	0.02	0.02	0.02	0.03
σ	all	0.06	0.07	0.26	0.20	0.07	0.22	0.07	0.06	0.12	0.09	0.13	0.09	0.06	0.13	0.11	0.11	0.18

¹Estimated evolutionary state: a \equiv AGB, r \equiv RGB, r+t \equiv RGB and tip, all \equiv all stars.

²“II” means [Fe/H] derived from Fe II lines or [eI/Fe] ratios referred to the Fe II metallicity values; “I” means these same quantities but employing the Fe I lines.

Table 9. Mean Abundances in M5, M4, and the Halo Field

Abundance	$\langle \text{field} \rangle^1$	$\langle \text{M5} \rangle$	σ	$\langle \text{M4} \rangle$	σ
[Mg/Fe]	+0.36	+0.34	0.07	+0.42	0.08
[Si/Fe]	+0.36	+0.31	0.07	+0.57	0.08
[Ca/Fe]	+0.27	+0.26	0.06	+0.25	0.11
[Ti/Fe]	+0.26	+0.22	0.09	+0.29	0.06
[V/Fe]	+0.02	-0.10	0.13	-0.05	0.06
[Ni/Fe]	-0.01	-0.05	0.06	+0.07	0.04
[Ba/Fe]	+0.09	+0.16	0.13	+0.56	0.10
[La/Fe]	-0.11	+0.02	0.11	+0.45	0.10
[Eu/Fe]	+0.42	+0.43	0.11	+0.34	0.10
Proton-Capture Elements					
[Na/Fe]	-0.10	+0.11	0.21	+0.23	0.22
[Al/Fe]	+0.24	+0.44	0.23	+0.63	0.14

¹Mean abundances for field stars with $[\text{Fe}/\text{H}] = -1.2$; see §8 for further explanation.

TABLE 10
THE ATOMIC LINE LIST

Species	λ Å	χ eV	$\log gf$	Ref.	Species	λ Å	χ eV	$\log gf$	Ref.
[O I]	6300.31	0.00	-9.75	1	Fe I	6159.38	4.61	-1.97	5
[O I]	6363.79	0.02	-10.25	1	Fe I	6165.36	4.14	-1.47	1
Na I	5682.63	2.10	-0.70	1	Fe I	6213.43	2.22	-2.66	4
Na I	5688.21	2.10	-0.46	1	Fe I	6219.28	2.20	-2.44	2
Na I	6154.23	2.10	-1.56	1	Fe I	6226.74	3.88	-2.22	1
Na I	6160.75	2.10	-1.26	1	Fe I	6229.23	2.84	-3.00	1
Mg I	5528.42	4.35	-0.36	2	Fe I	6240.66	2.22	-3.23	1
Mg I	5711.09	4.34	-1.63	1	Fe I	6246.32	3.60	-0.88	3
Al I	6696.03	3.14	-1.57	1	Fe I	6280.62	0.86	-4.37	1
Al I	6698.67	3.14	-1.89	1	Fe I	6290.97	4.73	-0.76	1
Si I	5793.08	4.93	-2.06	7	Fe I	6297.80	2.22	-2.74	1
Si I	6142.49	5.62	-1.48	1	Fe I	6301.50	3.65	-0.72	1
Si I	6145.02	5.61	-1.37	1	Fe I	6302.49	3.69	-1.15	1
Si I	6244.48	5.61	-1.27	1	Fe I	6311.51	2.83	-3.22	1
Si I	6243.82	5.61	-1.27	1	Fe I	6355.04	2.84	-2.29	1
Ca I	5590.12	2.51	-0.71	8	Fe I	6358.69	0.90	-4.47	2
Ca I	5867.56	2.92	-1.57	8	Fe I	6380.75	4.19	-1.40	1
Ca I	6161.30	2.52	-1.27	1	Fe I	6419.96	4.73	-0.24	1
Ca I	6166.44	2.52	-1.14	1	Fe I	6421.35	2.28	-1.94	1
Ca I	6169.04	2.52	-0.80	1	Fe I	6430.85	2.18	-2.00	2
Ca I	6169.56	2.52	-0.48	1	Fe I	6494.98	2.40	-1.24	16
Ca I	6455.60	2.52	-1.29	1	Fe I	6498.94	0.96	-4.69	1
Ca I	6471.66	2.51	-0.69	8	Fe I	6574.23	0.99	-5.02	1
Ca I	6499.65	2.52	-0.82	1	Fe I	6593.88	2.44	-2.42	2
Ca I	6508.84	2.51	-2.41	8	Fe I	6609.12	2.56	-2.69	14
Sc II	5526.82	1.77	+0.03	4	Fe I	6733.15	4.64	-1.43	15
Sc II	6245.62	1.51	-1.07	9	Fe I	6750.15	2.42	-2.62	14
Sc II	6279.74	1.50	-1.16	1	Fe II	6149.25	3.89	-2.72	1
Sc II	6309.90	1.50	-1.52	1	Fe II	6369.46	2.89	-4.25	1
Ti I	5866.45	1.07	-0.84	10	Fe II	6416.93	3.89	-2.79	1
Ti I	5922.11	1.05	-1.47	10	Fe II	6432.68	2.89	-3.71	4
Ti I	5965.83	1.88	-0.41	11	Fe II	6456.39	3.90	-2.08	1
Ti I	5978.54	1.87	-0.50	11	Fe II	6516.08	2.89	-3.45	1
Ti I	6064.63	1.05	-1.94	10	Ni I	6175.37	4.09	-0.53	1
Ti I	6126.22	1.07	-1.42	12	Ni I	6176.82	4.09	-0.53	1
Ti I	6303.77	1.44	-1.57	1	Ni I	6177.25	1.83	-3.50	1
Ti I	6312.24	1.46	-1.55	1	Ni I	6223.99	4.10	-0.99	2
Ti II	6606.97	2.06	-2.79	13	Ni I	6378.26	4.15	-0.89	1
V I	6274.66	0.27	-1.69	1	Ni I	6586.33	1.95	-2.81	9
V I	6285.16	0.28	-1.56	1	Ni I	6643.64	1.68	-2.01	4
Mn I	6021.79	3.08	+0.03	9	Ni I	6767.78	1.83	-2.17	9
Fe I	5501.48	0.96	-3.05	2	Ba II	5853.69	0.60	-1.01	6
Fe I	5506.79	0.99	-2.79	4	Ba II	6141.73	0.70	-0.08	1
Fe I	5522.45	4.21	-1.40	14	Ba II	6496.91	0.60	-0.38	1
Fe I	5560.21	4.43	-1.04	14	La II	5808.31	0.00	-2.34	17
Fe I	5586.77	3.37	-0.14	4	La II	6390.49	0.30	-1.41	18
Fe I	6079.01	4.65	-0.97	15	La II	6774.33	0.13	-1.75	17
Fe I	6151.62	2.18	-3.37	1	Eu II	6645.13	1.37	+0.20	1
Fe I	6157.73	4.07	-1.26	1					

REFERENCES.—1. Kraft et al. (1998) 2. Sneden et al. (1997); 3. Sneden et al. (1992; S92-M5); 4. Langer et al. (1998); 5. Kraft et al. (1995); 6. Sneden et al. (2000); 7. Garz (1973); 8. Drake et al. (1994); 9. Gonzalez & Lambert (1997); 10. Blackwell et al. (1982); 11. Blackwell et al. (1986); 12. Blackwell et al. (1983); 13. Martin et al. (1988); 14. Lambert et al. (1996); 15. Fuhr et al. (1988); 16. Thévenin (1990); 17. Brown & Wallerstein (1992) 18. Lawler et al (2001)

Table 11. Abundances for Keck Stars: Results from a Traditional Analysis

Star	Evol. ¹	Fe I ²	Fe II ²	<Fe> ³	O ⁴	Na	Mg	Al	Si	Ca	Sc	Ti	V	Mn	Ni	Ba	La	Eu
I-55	a	6.04	6.05	-1.48	-0.33	+0.29	...	+0.84	+0.33	+0.27	+0.03	+0.18	-0.39	-0.43	-0.02	+0.34	-0.05	+0.24
III-53	a	6.05	6.07	-1.46	-0.34	+0.38	...	+0.78	+0.36	+0.23	-0.01	+0.12	-0.45	-0.37	-0.08	+0.45	-0.02	+0.44
IV-26	a	6.13	6.11	-1.40	+0.17	-0.10	...	+0.20	+0.28	+0.35	-0.01	+0.11	...	-0.30	-0.08	+0.40	-0.08	+0.46
IV-30	a	6.07	6.09	-1.44	+0.03	+0.18	...	+0.54	+0.31	+0.25	+0.08	+0.18	-0.16	-0.34	-0.03	+0.33	-0.03	+0.37
III-18	a	6.06	6.07	-1.46	+0.16	+0.10	...	+0.42	+0.30	+0.29	+0.02	+0.16	-0.05	-0.26	-0.03	+0.28	-0.18	+0.27
I-20	a	6.05	6.05	-1.47	+0.34	+0.33	...	+0.34	+0.48	+0.21	+0.08	+0.17	-0.24	-0.28	-0.05	+0.37	-0.18	+0.36
IV-4 ⁵	r	6.27	6.28	-1.25	+0.24	-0.19	...	+0.22	+0.20	+0.36	+0.14	+0.16	-0.16	-0.35	+0.02	+0.45	+0.30	+0.25
IV-36	r	6.22	6.20	-1.30	+0.03	+0.19	...	+0.52	+0.28	+0.32	+0.21	+0.20	-0.01	-0.24	-0.06	+0.35	+0.07	+0.58
III-59	r	6.21	6.21	-1.31	-0.13	+0.22	...	+0.65	+0.29	+0.36	-0.10	+0.29	-0.11	-0.16	-0.07	+0.22	+0.13	+0.45
I-50	r	6.18	6.16	-1.35	-0.36	+0.45	...	+0.78	+0.24	+0.37	+0.09	+0.20	-0.08	-0.17	-0.03	+0.25	+0.10	+0.49
II-50	r	6.24	6.24	-1.28	+0.23	-0.01	...	+0.33	+0.25	+0.29	+0.03	+0.18	-0.17	-0.20	-0.14	+0.28	+0.15	+0.45
III-52	r	6.19	6.17	-1.34	+0.41	-0.21	...	+0.02	+0.28	+0.35	+0.07	+0.24	+0.05	-0.21	-0.02	+0.24	+0.10	+0.55
II-74	r	6.27	6.25	-1.25	-0.24	+0.27	...	+0.66	+0.31	+0.30	+0.20	+0.13	-0.13	-0.15	-0.07	+0.31	+0.08	+0.49
I-2	r	6.17	6.14	-1.36	+0.08	+0.29	...	+0.50	+0.34	+0.38	+0.10	+0.27	-0.12	-0.25	-0.07	+0.20	+0.05	+0.46
II-59 ⁵	r	6.29	6.25	-1.25	-0.06	+0.36	...	+0.64	+0.29	+0.41	+0.12	+0.27	-0.08	-0.31	-0.07	+0.01	+0.17	+0.36
I-61	r	6.22	6.21	-1.30	+0.32	-0.16	...	+0.10	+0.27	+0.34	+0.09	+0.23	-0.02	-0.18	-0.08	+0.28	+0.16	+0.57
I-58	r	6.21	6.22	-1.31	+0.03	+0.29	...	+0.55	+0.30	+0.37	+0.13	+0.22	-0.05	-0.16	-0.04	+0.25	+0.04	+0.41
IV-34	r	6.20	6.20	-1.32	+0.17	+0.13	...	+0.38	+0.28	+0.32	+0.07	+0.27	-0.07	-0.20	-0.05	+0.25	-0.13	+0.43
I-14	r	6.19	6.20	-1.33	+0.17	+0.17	...	+0.53	+0.32	+0.28	+0.17	+0.20	-0.09	-0.20	-0.07	+0.18	+0.14	+0.45
III-149	t	6.20	6.18	-1.33	+0.36	-0.13	...	+0.11	+0.27	+0.32	+0.05	+0.24	0.00	-0.19	-0.07	+0.22	+0.01	+0.50
IV-19	t	6.11	6.15	-1.39	+0.36	+0.06	...	+0.35	+0.34	+0.30	+0.09	+0.29	-0.02	-0.21	-0.02	+0.19	+0.11	+0.54
IV-81	t	6.11	6.14	-1.39	+0.28	+0.19	...	+0.43	+0.34	+0.30	+0.08	+0.33	+0.01	-0.13	-0.08	+0.17	+0.11	+0.46
IV-47	t	6.15	6.17	-1.36	+0.17	+0.25	+0.34	+0.25	+0.34	+0.31	+0.09	+0.35	+0.14	...	-0.02	+0.23	+0.16	+0.46
II-85	t	6.18	6.20	-1.33	+0.28	+0.40	+0.33	+0.04	+0.33	+0.30	+0.01	+0.26	+0.06	...	-0.04	+0.11	+0.12	+0.45
G2	t	6.16	6.18	-1.35	+0.26	+0.22	...	+0.40	+0.26	+0.31	+0.03	+0.47	-0.06	0.00	-0.04	+0.20	+0.02	+0.45

Mean Abundances by Evolutionary State																		
<>	a	6.07	6.07	-1.45	+0.01	+0.20	...	+0.52	+0.34	+0.27	+0.03	+0.15	-0.26	-0.33	-0.05	+0.36	-0.09	+0.36
σ	a	0.03	0.02	0.03	0.28	0.18	...	0.25	0.07	0.05	0.04	0.03	0.16	0.06	0.03	0.06	0.07	0.09
<>	r	6.22	6.21	-1.30	+0.07	+0.14	...	+0.45	+0.28	+0.34	+0.10	+0.22	-0.09	-0.21	-0.06	+0.25	+0.10	+0.46
σ	r	0.04	0.04	0.04	0.22	0.22	...	0.23	0.04	0.04	0.08	0.05	0.06	0.06	0.04	0.10	0.10	0.09
<>	r+t	6.20	6.20	-1.32	+0.14	+0.15	+0.34	+0.42	+0.27	+0.33	+0.09	+0.25	-0.07	-0.19	-0.05	+0.23	+0.10	+0.46
σ	r+t	0.05	0.04	0.04	0.21	0.20	0.01	0.22	0.07	0.04	0.07	0.08	0.06	0.08	0.03	0.09	0.09	0.09
<>	all	6.17	6.17	-1.35	+0.11	+0.16	+0.34	+0.45	+0.29	+0.32	+0.07	+0.23	-0.10	-0.23	-0.05	+0.26	+0.05	+0.44
σ	all	0.08	0.07	0.07	+0.23	+0.19	0.01	+0.22	+0.07	+0.05	+0.07	0.08	0.13	0.09	0.03	0.10	0.12	0.09

¹Estimated evolutionary state: a \equiv AGB, r \equiv RGB, t \equiv RGB tip, all \equiv all stars.

²Absolute abundances $\log \epsilon(\text{Fe})$ derived from Fe I and Fe II lines.

³The mean $[\text{Fe}/\text{H}]$ values derived from unweighted averages of abundances derived from Fe I and Fe II lines.

⁴For this and all remaining columns, the element symbols "X" refer to $[\text{X}/\text{Fe}]$ values, using the mean $[\text{Fe}/\text{H}]$ ratios.

⁵Abundances for II-59 and IV-4 have low weight; their spectra have $S/N < 50$.